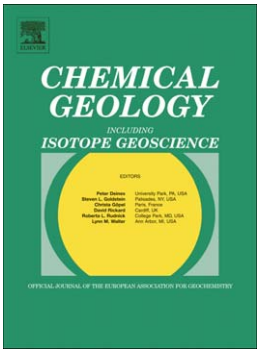

U-Pb and Th-Pb dating of apatite by LA-ICPMS

David M. Chew, Paul J. Sylvester, Mike N. Tubrett

PII: S0009-2541(10)00403-1
DOI: doi: 10.1016/j.chemgeo.2010.11.010
Reference: CHEMGE 16086

To appear in: *Chemical Geology*

Received date: 6 July 2010
Revised date: 4 November 2010
Accepted date: 5 November 2010

Please cite this article as: Chew, David M., Sylvester, Paul J., Tubrett, Mike N., U-Pb and Th-Pb dating of apatite by LA-ICPMS, *Chemical Geology* (2010), doi: 10.1016/j.chemgeo.2010.11.010

U-Pb and Th-Pb dating of apatite by LA-ICPMS

David M. Chew [a,*]
Paul J. Sylvester [b]
Mike N. Tubrett [b]

[a] Department of Geology, School of Natural Sciences, Trinity College Dublin, Dublin 2, Ireland
[b] Department of Earth Sciences and Inco Innovation Centre, Memorial University, St. John's, Newfoundland, A1B 3X5 Canada

[*] Corresponding author. Department of Department of Geology, School of Natural Sciences, Trinity College Dublin, Dublin 2, Ireland.
Tel.: +353 1 8963481; fax: +353 1 6711199, Email address: chewd@tcd.ie (David M. Chew).

Abstract

Apatite is a common U- and Th-bearing accessory mineral in igneous and metamorphic rocks, and a minor but widespread detrital component in clastic sedimentary rocks. U-Pb and Th-Pb dating of apatite has potential application in sedimentary provenance studies, as it likely represents first cycle detritus compared to the polycyclic behaviour of zircon. However, low U, Th and radiogenic Pb concentrations, elevated common Pb and the lack of a U-Th-Pb apatite standard remain significant challenges in dating apatite by LA-ICPMS, and consequently in developing the chronometer as a provenance tool.

This study has determined U-Pb and Th-Pb ages for seven well known apatite occurrences (Durango, Emerald Lake, Kovdor, Mineville, Mudtank, Otter Lake and Slyudyanka) by LA-ICPMS. Analytical procedures involved rastering a 10μm spot over a 40×40μm square to a depth of 10μm using a Geolas 193nm ArF excimer laser coupled to a Thermo ElementXR single-collector ICPMS. These raster conditions minimized laser-induced inter-element fractionation which was corrected for using the back-calculated intercept of the time-resolved signal. A Tl–U–Bi–Np tracer solution was aspirated with the sample into the plasma to correct for instrument mass bias. External standards (Plešovice and 91500 zircon, NIST SRM 610 and 612 silicate glasses and STDP5 phosphate glass) along with Kovdor apatite were analysed to monitor U-Pb, Th-Pb and Pb-Pb ratios.

Common Pb correction employed the ^{207}Pb method, and also a ^{208}Pb correction method for samples with low Th/U. The ^{207}Pb and ^{208}Pb corrections employed either the initial Pb isotopic composition where known or the Stacey and Kramers model, and propagated conservative uncertainties in the initial Pb isotopic composition. Common Pb correction using the Stacey and Kramers (1975) model employed an initial Pb isotopic composition calculated from either the estimated U-Pb age of the sample or an iterative approach. The age difference between these two methods is typically less than 2%, suggesting that the iterative approach works well for samples where there are no constraints on the initial Pb composition, such as a detrital sample. No ^{204}Pb correction was undertaken because of low ^{204}Pb counts on single collector instruments and ^{204}Pb interference by ^{204}Hg in the argon gas supply.

Age calculations employed between 11 and 33 analyses per sample and used a weighted average of the common Pb-corrected ages, a Tera-Wasserburg Concordia intercept age and a Tera–Wasserburg Concordia intercept age anchored through

common Pb. The samples in general yield ages consistent (at the 2σ level) with independent estimates of the U-Pb apatite age, which demonstrates the suitability of the analytical protocol employed. Weighted mean age uncertainties are as low as 1-2% for U- and / or Th-rich Palaeozoic-Neoproterozoic samples; the uncertainty on the youngest sample, the Cenozoic (31.44 Ma) Durango apatite, ranges from 3.7–7.6% according to the common Pb-correction method employed. The accurate and relatively precise common Pb-corrected ages demonstrate the U-Pb and Th-Pb apatite chronometers are suitable as sedimentary provenance tools. The Kovdor carbonatite apatite is recommended as a potential U-Pb and Th-Pb apatite standard as it yields precise and reproducible ^{207}Pb-corrected, ^{232}Th-^{208}Pb, and common Pb-anchored Tera-Wasserburg Concordia intercept ages.

Keywords

U-Pb; Th-Pb; geochronology; apatite; LA-ICPMS; common Pb; provenance

1. Introduction

Apatite is a common accessory mineral in igneous, metamorphic and clastic sedimentary rocks. It is a nearly ubiquitous accessory phase in igneous rocks, due in part to the low solubility of P_2O_5 in silicate melts and the limited amount of phosphorus incorporated into the crystal lattices of the major rock-forming minerals (Piccoli and Candela, 2002). Apatite is common in metamorphic rocks of pelitic, carbonate, basaltic, and ultramafic composition and is found at all metamorphic grades from transitional diagenetic environments to migmatites (Spear and Pyle, 2002). Apatite is also virtually ubiquitous in clastic sedimentary rocks (Morton and Hallsworth, 1999).

Apatite is widely employed in low-temperature thermochronology studies with the apatite fission track and apatite (U-Th)/He thermochronometers yielding thermal history information in the 60 - 120°C (Laslett et al., 1987) and 55 - 80°C (Farley, 2000) temperature windows respectively. Apatite has also been employed in high-temperature thermochronology studies which demonstrate that the U-Pb apatite system has a closure temperature of ca. 450 – 550°C (Chamberlain and Bowring, 2000; Schoene and Bowring, 2007). Apatite has also been employed in Lu-Hf geochronology studies (Barfod et al., 2003) and as an Nd isotopic tracer (Foster and Vance, 2006; Gregory et al., 2009).

Apatite has been widely used in detrital thermochronology studies (Bernet and Speigel, 2004), and potentially has broad application as a sedimentary provenance tool. Firstly, several analytical techniques (e.g., fission track, (U-Th)/He or Nd isotopes) can in principle be undertaken on the same apatite grain (e.g., Carter and Foster, 2009). Secondly, compared to the well documented polycyclic behaviour of the stable heavy mineral zircon, apatite is unstable in acidic groundwaters and weathering profiles and has only limited mechanical stability in sedimentary transport systems (Morton and Hallsworth, 1999). It therefore likely represents first cycle detritus, and would yield complementary information to zircon provenance studies. Zircon provenance studies have been revolutionised in the last decade by the advent of the LA-ICPMS U-Pb method, which offers low-cost, rapid data acquisition and sample throughput compared to the ID-TIMS or ion microprobe U-Pb methods (e.g., Košler and Sylvester, 2003). However, even though it is also a U-bearing accessory phase, there are few studies which demonstrate the applicability of the LA-ICPMS U-

Pb apatite chronometer by dating apatite standards of known crystallization age. This study has determined LA-ICPMS U-Pb and Th-Pb ages for seven well known apatite occurrences and one apatite sample of unknown age, with the aim of developing the U-Pb and Th-Pb apatite chronometers as a sedimentary provenance tool.

1.1 The problem of common Pb correction in U-Th-Pb dating of apatite

Precise U-Pb and Th-Pb apatite age determinations are commonly hindered by low U, Th and Pb concentrations and high common Pb / radiogenic Pb ratios which usually necessitate common Pb correction. Although high-precision, low-blank ID-TIMS analysis can partially circumvent the problem of low parent and daughter isotope contents, common Pb correction remains a major drawback in U-Pb apatite chronometry. Apatite can accommodate a significant amount of initial Pb in its crystal structure and as a consequence one of the main limitations on the accuracy and precision of apatite age determinations is the need to use either i) Concordia or isochron plots on a suite of cogenetic apatite grains with a large spread in common Pb / radiogenic Pb ratio or ii) to undertake a Pb correction based on an appropriate choice of initial Pb isotopic composition.

i) There exist a variety of methods that do not require an estimate of the initial Pb isotopic composition. They typically require several analyses of a suite of cogenetic apatite grains with a significant spread in common Pb / radiogenic Pb ratios to define a well constrained linear array on a Concordia diagram or isochron. The Total-Pb/U isochron, a three-dimensional $^{238}U/^{206}Pb$ vs. $^{207}Pb/^{206}Pb$ vs. $^{204}Pb/^{206}Pb$ plot (Ludwig, 1998), yields the smallest error of any possible U/Pb or Pb/Pb isochron as all relevant isotope ratios are used at the same time. Discordance and variation in the initial Pb composition of the suite of analysed grains on a Total-Pb/U isochron can also be assessed by the MSWD of the regression. Other isochrons, such as the $^{238}U/^{204}Pb$ vs. $^{206}Pb/^{204}Pb$, $^{235}U/^{204}Pb$ vs. $^{207}Pb/^{204}Pb$, $^{232}Th/^{204}Pb$ vs. $^{208}Pb/^{204}Pb$ and $^{207}Pb/^{204}Pb$ vs. $^{206}Pb/^{204}Pb$ plots assume the U-Pb* data (where Pb* = the radiogenic Pb component) are concordant to calculate accurate isochron dates, which can be difficult to assess but can be evaluated to some extent by the MSWD of the regression. Another approach often employed in U-Pb dating of high common Pb phases, such as the LA-ICPMS U-Pb dating studies of perovskite (Cox and Wilton, 2006) and titanite (Simonetti et al., 2006) involves projecting an intercept through the uncorrected data

on a Tera–Wasserburg Concordia to determine the common Pb-component (*y*-intercept) on the $^{207}Pb/^{206}Pb$ axis. The $^{238}U/^{206}Pb$ age can then be calculated as either a lower intercept age on the $^{238}U/^{206}Pb$ axis (x-intercept) or as a weighted average of ^{207}Pb-corrected ages (see below) using the Concordia $^{207}Pb/^{206}Pb$ intercept as an estimate of the initial Pb isotopic composition. This approach also assumes that the U-Pb* data are concordant and equivalent.

ii) The second set of approaches involves correcting for initial Pb. Three methods are commonly employed in the literature, the ^{204}Pb-, ^{207}Pb- and ^{208}Pb-correction methods (e.g., Williams, 1998). The mathematical details of how these approaches are applied are described in Appendix A. Estimates of initial Pb isotopic compositions are typically derived from Pb evolution models (e.g., Stacey and Kramers, 1975) or by analysing a low-U co-magmatic phase (e.g., K-feldspar or plagioclase) which exhibits negligible in-growth of radiogenic Pb.

The ^{204}Pb correction method is potentially the most powerful as it does not assume U/Pb* concordance. It does however require accurate measurement of ^{204}Pb and is also sensitive to the low $^{206}Pb/^{204}Pb$ ratios encountered in Phanerozoic samples (e.g., Cocherie et al., 2009). It is thus ideally suited to U-Pb dating by high-precision ID-TIMS, as low ^{204}Pb concentrations can be measured accurately. Additionally the ^{204}Pb method preserves one of the strengths of the U–Pb system, which is the ability to identify concordance of the ^{204}Pb-corrected data. However potential discordance can be obscured by an inappropriate choice of initial Pb (e.g., by using Pb evolution models). An alternative approach involves analysing a co-existing phase with a low U/Pb ratio (μ), such as K-feldspar or plagioclase, which preserves the initial Pb isotopic composition at the time of apatite crystallization (e.g., Chamberlain and Bowring, 2000; Schoene and Bowring, 2007), although this approach is often not feasible for the analysis of detrital minerals and minerals in complex metamorphic rocks where isotopic equilibrium between phases cannot be assumed.

Both the ^{207}Pb- and ^{208}Pb-correction methods assume initial concordance in $^{238}U/^{206}Pb$ - $^{207}Pb/^{206}Pb$ and $^{238}U/^{206}Pb$ - $^{208}Pb/^{232}Th$ space respectively. The ^{207}Pb-correction method is commonly used in U-Pb ion microprobe studies (Gibson and Ireland, 1996), and only requires precisely measured $^{238}U/^{206}Pb$ and $^{207}Pb/^{206}Pb$ ratios and an appropriate choice of common Pb. The ^{208}Pb-correction method is less commonly applied. It requires the measurement of $^{208}Pb/^{206}Pb$ and $^{232}Th/^{238}U$ and an

appropriate choice of initial $^{208}Pb/^{206}Pb$, and works well for samples with low Th/U (e.g., < 0.5) (Appendix A; Cocherie, 2009; Williams 1998).

1.2 U-Th-Pb apatite dating by LA-ICPMS

In addition to the problem of incorporation of common Pb into the apatite crystal lattice, U-Th-Pb dating by LA-ICPMS also presents the problem of laser-induced U-Th-Pb fractionation. A matrix-matched standard is usually required for external calibration of down-hole fractionation of Pb, Th and U in LA-ICPMS dating of accessory minerals because different minerals (e.g., apatite, titanite and zircon) typically show different time-resolved Pb/U and Pb/Th signals during ablation (e.g., Gregory et al. 2007).

Few studies have undertaken U-Pb apatite dating by LA-ICPMS. $^{207}Pb–^{206}Pb$ dating of apatite has been conducted on Paleoproterozoic samples with good precision (0.3% 2SE on individual analyses) and accuracy by multi-collector LA-ICP-MS (Willigers et al., 2002). Common Pb correction either employed Pb isotopic analysis of coexisting plagioclase or utilized isochron calculations where there was sufficient Pb isotopic heterogeneity on replicate analyses of single crystals. Although it does away with the need to correct for laser-induced U-Th-Pb fractionation, Pb-Pb dating removes the ability to evaluate concordance and is of limited application to dating Phanerozoic apatites due to the difficulty in obtaining precise $^{207}Pb–^{206}Pb$ ratios from young samples.

Storey et al. (2006) dated Paleoproterozoic apatite mineralization hosted by intermediate to acid volcanic rocks of the Norrbotten iron ore province in northern Sweden by quadrupole ICP-MS. Common Pb was monitored by analysing ^{204}Pb and was sufficiently low in this sample suite as to not necessitate a common Pb correction. U/Pb ratios in apatite were corrected using the zircon geostandard 91500 (Wiedenbeck et al., 1995). The U-Pb apatite ages were mostly moderately reversely discordant which was attributed to possible elemental fractionation of Pb and U isotopes relative to the external standard during laser ablation.

Carrapa et al. (2009) dated detrital apatite from the Cenozoic Salar de Pastos Grandes and Arizaro basins of the central Andean Puna plateau by multi-collector ICPMS. U/Pb laser-induced fractionation was constrained by analysis of Bear Lake Road titanite (quoted age of 1050 ± 1 Ma), a Sri Lanka zircon crystal (563.5 ± 3.2 Ma,

Gehrels et al., 2008) and NIST SRM 610 trace element glass ($^{206}Pb/^{238}U$ = 0.2565, Stern and Amelin, 2003). Common Pb correction employed the measured ^{204}Pb assuming an initial Pb composition from Stacey and Kramers (1975).

However, there are presently no studies that demonstrate the applicability of the LA-ICPMS U-Th-Pb apatite chronometer by dating apatite standards of known crystallization age, which is the focus of this study. The ultimate aim is to develop the U-Pb and Th-Pb apatite chronometers for use in sedimentary provenance studies. Hence analytical procedures and common Pb corrections, which are described in section 3, are optimised for single analyses of small apatite grains.

2. Apatite samples

This study has determined U-Pb and Th-Pb ages for seven well known apatite occurrences (Durango, Emerald Lake, Kovdor, Mineville, Mudtank, Otter Lake and Slyudyanka) along with one apatite sample of unknown age. All seven apatite occurrences along with the sample of unknown age have independent temporal constraints on the timing of apatite crystallization which are summarized below and in Table 1. The apatites in all seven occurrences are megacrysts (typically prisms several cm long and at least 1 cm in diameter). Closure temperatures were calculated using the program Closure (Brandon et al., 1998) for the apatite megacrysts (minimum radius a = 0.5 cm) with a pre-exponential coefficient (D_0) = 2×10^{-4} cm^2/s and an activation energy (E) = 231.5 kJ/mol (Cherniak et al. (1991). This yields closure temperatures of ca. 640 ºC for a cooling rate of 1 ºC / Ma and ca. 790 ºC for a cooling rate of 100 ºC / Ma. Sample DC 4/5/2 has a mean grain radius of ca. 100 microns, yielding closure temperatures estimates of ca. 460 ºC for a cooling rate of 1 ºC / Ma and ca. 550 ºC for a cooling rate of 100 ºC / Ma.

2.1 Durango apatite

The Durango apatite is a distinctive yellow-green fluorapatite that is found as exceptional coarse crystals within the open pit iron mine at Cerro de Mercado, on the northern outskirts of Durango City, Mexico. It is a widely available and widely used mineral standard in apatite fission-track and (U–Th)/He dating and apatite electron micro-probe analyses. More details on the deposit are available in McDowell et al.

(2005) and are summarised here. The apatite is associated with emplacement of small felsic intrusions along the southern margin of the Chupaderos caldera complex, and formed between the eruptions of two major ignimbrites from the caldera. Four single-crystal sanidine-anorthoclase ^{40}Ar–^{39}Ar ages from these ignimbrites have yielded a reference age of 31.44 ± 0.18 Ma (2σ) for the apatite itself (McDowell et al., 2005, Table 1). 24 (U–Th–Sm)/He ages yield a mean of age of 31.02 ± 1.01 (1σ), with a mean U/Th (wt/wt) ratio of 0.054 calculated from 30 analyses (McDowell et al., 2005).

2.2 Emerald Lake apatite

Coulson et al. (2002) present a detailed petrological and chemical study of the mid-Cretaceous, composite Emerald Lake pluton, which crops out in the northern Canadian Cordillera in the Yukon Territory. It was intruded as a series of magmatic pulses which produced a strong petrological zonation from augite syenite, hornblende quartz syenite and monzonite, to biotite granite. Apatite is an accessory mineral in the syenite, monzonite and granite. The U-Pb and ^{40}Ar–^{39}Ar geochronological study of Coulson et al. (2002) is summarised in Table 1. The oldest age is a 94.5 ± 0.2 Ma U-Pb zircon age from a syenite, while the youngest age is a 92.2 ± 0.9 Ma U-Pb titanite age from a granite. The titanite age of 92.2 ± 0.9 Ma is adopted for the Emerald Lake apatite (Table 1).

2.3 Kovdor carbonatite apatite

The ca. 40 km^2 Kovdor massif is part of the Palaeozoic Kola Alkaline Province, which consists of more than twenty-four intrusive complexes of Devonian age (Kramm et al., 1993). The Kovdor massif is an economically important ultrabasic-alkaline complex which exhibits a wide compositional range of magmatic and metasomatic rocks. Two components of the complex, phoscorites and carbonatites, have been the subject of a detailed geochronological study using several isotopic systems (U-Pb, Th-Pb and Rb-Sr) on various phases (baddeleyite, zircon, apatite, phlogopite) (Amelin and Zaitsev, 2002). More details on the Kovdor carbonatite are available in Amelin and Zaitsev (2002) and references therein. Amelin and Zaitsev (2002) analysed apatite from six phoscorite and three carbonatite samples, with U and

Th contents ranging from 0.2 to 3.6 ppm and 62 to 150 ppm respectively. Co-existing low-U calcite was used to constrain the initial Pb isotopic composition of the apatite. A total Pb/U isochron of all apatite and calcite analyses yielded an age of 380.6 ± 2.6 Ma (MSWD = 38), while a regression of apatite analyses only yielded a total Pb/U isochron of 377.5 ± 3.5 Ma (MSWD = 27), which is the reference age adopted in this study (Table 1). In a global study which analysed over 700 apatite grains from a range of rock types to investigate the potential usefulness of apatite as an indicator mineral in mineral exploration, Belousova et al. (2002) found the highest Th values (over 2000 ppm) in apatite from the Kovdor carbonatite.

2.4 Mineville apatite

The Kiruna-type Fe-REE deposit at Mineville, Essex County, New York State is hosted by the Lyon Mountain gneiss and contains magnetite, hematite, apatite, stillwellite-Ce, fluorian edenite, ferro-actinolite, titanite, zircon and allanite in the main ore bodies (Lupulescu and Pyle, 2005). The host rock and ore bodies commonly exhibit the same tectonic fabrics and layering. Foose and McLelland (1995) interpret the Lyon Mountain gneiss as a late- to post-tectonic intrusive suite emplaced during the waning stages of the Ottowan orogeny, although other authors favour a pre-tectonic, volcanic protolith for the host rocks (Whitney and Olmsted, 1988; Whitney, 1996). U-Pb zircon determinations from weakly to undeformed rocks in the Lyon Mountain gneiss yield ages of ca. 1048 and 1035 Ma, respectively, while an undeformed, cross-cutting pegmatite yields a U-Pb zircon age of ca. 1035 Ma (McLelland and Foose, 1996). These results demonstrate that regional Ottowan deformation ended in the Adirondacks by ca. 1040 Ma. Several U/Pb garnet and sphene ages from this region cluster in the 1030 – 990 Ma age range and are interpreted as metamorphic ages while metamorphic rutile ages cluster at ca. 900 Ma (Mezger et al., 1991). Given the high closure temperatures for the Mineville apatite sample (c. 650 ºC for the cooing rate of 1.5 ºC / Ma quoted in Mezger et al., 1991) it likely records cooling shortly after the Ottowan thermal peak. The assumed U-Pb age of the Mineville apatite is thus relatively poorly constrained, and a reference age of 1040 – 990 Ma is adopted in this study (Table 1).

2.5 Mudtank apatite

Apatite megacrysts occur within the Mud Tank Carbonatite, in the Strangways Ranges of the Northern Territory NE of Alice Springs. A zircon U–Pb age of 732 ± 5 Ma and a whole-rock Rb–Sr age of 735 ± 75 Ma were reported by Black and Gulson (1978) while younger Rb–Sr biotite ages between 319 and 349 Ma were interpreted as representing overprinting during the Alice Springs Orogeny (Haines et al., 2001). A pooled apatite fission track age of 298 ± 23 Ma is just slightly younger than the biotite Rb–Sr ages suggesting rapid post-orogenic cooling (Green et al., 2006). The adopted age of the Mudtank apatite in Table 1 is taken as the oldest biotite age (349 Ma) from the study of Haines et al. (2001). The apatite fission track data demonstrate that the Mudtank apatite has a low U content of only 3.2 ppm.

2.6 Otter Lake (Yates Mine) apatite

The Otter Lake area, Québec, is located north of the Bancroft domain within the Grenville Province. The rocks of the Otter Lake area comprise marbles, gneisses, amphibolites, and skarns that underwent upper-amphibolite-facies metamorphism at temperatures and pressures of 650 to 700 °C and 6.5–7 kbar in connection with the Elzevirian and Ottowan phases of the Grenville orogeny (Kretz et al., 1999). Barfod et al. (2005) have dated apatite by the Lu-Hf and $^{207}Pb/^{206}Pb$ stepwise leaching methods from the Yates Mine locality in the Otter Lake region, where apatite specimens typically take the form of dark-green – brown, long hexagonal prisms with pyramidal terminations set in a hydrothermally altered, salmon-pink calcite matrix. Three apatite fractions from the Otter Lake apatite yield a single-crystal Lu-Hf isochron of 1042 ± 16 Ma (MSWD = 1.0). Combining analyses from this apatite and a titanite from the same area leads to a more precise Lu-Hf age of 1031 ± 6 Ma (MSWD = 1.7). $^{207}Pb/^{206}Pb$ stepwise leaching analyses from five HBr leaching steps and a bulk dissolution on an aliquot from the same crystal lie on an isochron of 913 ± 7 Ma (MSWD = 0.24) in $^{207}Pb/^{204}Pb$-$^{206}Pb/^{204}Pb$ space, which is the reference age adopted in this study (Table 1). Pb, Th and U concentration estimates by ICPMS are 74, 722 and 92 ppm respectively (Barfod et al., 2005).

2.7 Slyudyanka apatite

The Slyudyanka Complex is a granulite-facies supracrustal sequence which crops out on the southwest coast of Lake Baikal. The Slyudyanka Complex is dominated by metamorphosed siliceous–carbonate phosphorites, which are composed of apatite (from 1–2 to 60 wt %), quartz, diopside, calcite, forsterite and dolomite with minor retrograde tremolite (Reznitskii et al., 1998). Reznitskii et al. (1998) present $^{207}Pb/^{206}Pb$ apatite - whole rock isochrons of 465 ± 3 Ma (MSWD = 5.5) and 456 ± 18 Ma (MSWD = 1.3) corresponding to the age of high-grade metamorphism. A phlogopite-calcite-apatite paragenetic assemblage has yielded a Rb-Sr isochron age of 460 ± 7 Ma Reznitskii et al., 1999). This is further constrained by U-Pb zircon ages of 471 ± 1 Ma (Salnikova et al. 1998) and 447 ± 2 Ma (Reznitskii et al., 2000) from early syenites and monzonites and later 'post-phlogopitic' pegmatites respectively. Given the high closure temperatures for the Slyudyanka apatite megacrysts, a reference age of 460 Ma (corresponding to the timing of peak metamorphism) is adopted for Slyudyanka apatite in this study (Table 1). Dempster et al. (2003) present Th and U concentrations of 111.4 and 61.4 ppm respectively for Slyudyanka apatite.

2.8 Sample DC 4/5/2

In contrast to the other dated samples which were large, single crystal specimens, sample DC 4/5/2 was a pure apatite separate with a mean grain size of ca. 200 µm. It thus has a much lower closure temperature (c. 460 ºC for a cooling rate of 1 ºC / Ma and ca. 550 ºC for a cooling rate of 100 ºC / Ma) compared to the megacrysts dated in this study. It was selected to investigate the spread in U / total Pb ratios in apatites on the scale of a large hand specimen (c. 5 kg). The sample is a strongly-foliated granodiorite (termed the Sitabamba orthogneiss) which intrudes Lower Palaeozoic metasedimentary rocks in the Eastern Cordillera of Peru (Chew et al., 2007). The crystallization of the granodioritic protolith of the Sitabamba orthogneiss has been constrained by a U-Pb TIMS zircon Concordia age of 442.4 ± 1.4 Ma and a LA-ICPMS U-Pb zircon Concordia age of 444.2 ± 6.4 Ma. It exhibits conspicuous augen of relic igneous plagioclase along with a metamorphic assemblage of garnet, biotite, muscovite, epidote and plagioclase. Thermobarometric estimates for the metamorphic assemblages are 700 ˚C and 12 kbar (Chew et al., 2005). Subsequent post-metamorphic rapid cooling is constrained by an unpublished $^{40}Ar–^{39}Ar$ biotite age of 394.6 ± 2 Ma. This biotite age is adopted as the age of this sample

(Table 1). LA-MC-ICPMS Pb analyses of K-feldspar from sample DC 4/5/2 yield $^{207}Pb/^{206}Pb$ and $^{208}Pb/^{206}Pb$ values of 0.857 ± 0.008 and 2.089 ± 0.023 respectively (Table 1).

2.9 Summary of the age constraints

Three of the apatite samples (Durango, Emerald Lake and Kovdor carbonatite apatite) have robust independent age constraints and simple post-crystallization histories (rapid thermal relaxation following magmatic emplacement). In addition, Kovdor carbonatite apatite is constrained by extremely high quality U-Th-Pb TIMS data (section 5.2) Three of the apatite samples (Slyudyanka, Otter Lake and Mineville apatite) have reasonable independent age constraints and more complicated thermal histories (cooling from an upper amphibolite- to granulite-facies metamorphic peak), but given the high closure temperatures of these apatite megacrysts (650 – 750 ºC) they are likely in many cases to be recording crystallisation or cooling shortly after the metamorphic peak. Two samples (Mudtank apatite and sample DC 4/5/2) have poor independent age and thermal history constraints.

3. Methods

3.1 Common Pb correction methods employed in this study

As the aim of this study is to develop the U-Pb and Th-Pb apatite chronometers as a sedimentary provenance tool, common Pb corrections and analytical procedures were optimised for single analyses of small apatite grains. No ^{204}Pb correction was undertaken in this study because of ^{204}Pb interference by ^{204}Hg in the argon gas supply. ^{204}Hg typically represented 75 – 95% of the 204 peak, and hence ^{204}Pb could not be measured accurately without using a prohibitively long dwell time on the 204 peak. Total-Pb/U isochrons (Ludwig, 1998) or ^{204}Pb correction were therefore not possible. Common Pb correction employed four separate approaches. These include the ^{207}Pb-correction method, and the ^{208}Pb-correction method for samples with low Th concentrations and Th/U < 5. The ^{207}Pb and ^{208}Pb corrections employed either the initial Pb isotopic composition where known, or used the Stacey and Kramers (1975) model for crustal Pb evolution. In both cases an uncertainty of

5% (2σ) was propagated on the initial $^{207}Pb/^{206}Pb$ and $^{208}Pb/^{206}Pb$ isotopic ratios to the final age calculation. The 5% uncertainty in initial Pb isotopic ratios is based on the North Atlantic Pb isotopic data compilation of Tyrrell et al. (2007) and the Andean Pb isotopic data compilation of Mamani et al. (2008). It is by necessity an approximation, but appears to capture the potential Pb isotopic variation in crustal provinces with varying Pb isotopic signatures and their deviation from the Stacey and Kramers (1975) Pb evolution model.

Common Pb correction also employed a Tera–Wasserburg Concordia approach. The variability in U / total Pb ratio of the uncorrected data was used to determine the common Pb-component on the $^{207}Pb/^{206}Pb$ axis and an intercept age on the $^{238}U/^{206}Pb$ axis, similar to the approach adopted by Cox and Wilton (2006) and Simonetti et al. (2006). It should be noted that this approach is not feasible for the analysis of detrital minerals which will have different initial $^{207}Pb/^{206}Pb$ isotopic compositions. The final approach also involved plotting the uncorrected data on a Tera-Wasserburg Concordia but the intercept was anchored through the initial Pb isotopic composition using either the Stacey and Kramer's model or independent constraints.

3.2 Laser-induced Pb / U fractionation correction employed in this study

Elemental fractionation is an important consideration in U-Pb dating of accessory minerals by LA-ICPMS. Several techniques have been used to both minimize this fractionation or to correct for it, primarily in U-Pb dating studies of zircon. The reader is referred to Košler and Sylvester (2003) for a detailed account of these techniques.

One approach to correcting elemental fractionation involves using an external standard of known age to derive an empirical correction factor that can be applied to the unknown sample (e.g., Jackson et al. 1996). Pb/U ratios of the standard are measured before and after analysis of the unknown, and a correction factor (ratio) between the true standard age and the measured age of the standard is calculated. The true age (Pb/U ratio) of the unknown can then be derived from the measured sample ratios using this correction factor. The data need also be corrected for instrument drift (change in sensitivity with time) prior to correction for elemental fractionation. This method assumes instrument parameters remain constant between analysis of the

standard and the unknown, and there are no significant matrix effects on the measured Pb/U and Pb isotopic ratios between the standard and the sample. As presently there are no well characterised U-Pb apatite standards, this approach was not adopted in this study. Elemental fractionation of Pb and U can also be corrected for by using empirical equations that describe the fractionation (e.g., Horn et al. 2000). This method assumes that for a given laser spot size and laser energy density, there is a linear relationship between the depth of the laser pit and the measured Pb/U ratio. It is therefore possible to derive an external fractionation correction based on empirical equations that quantify the fractionation slope for different spot sizes.

The final commonly used approach to correct for Pb/U elemental fractionation, and the approach adopted in this study, is that of Košler et al. (2002). This method is based on the premise of Sylvester and Ghaderi (1997) that laser-induced, volatile/refractory element fractionation is a linear function of time, and therefore it can be corrected by extrapolating the measured ratios back to the start of ablation. Pb/U ratios at the start of laser ablation therefore are biased only by the mass discrimination (bias) of the ICPMS instrument. The fractionation-corrected Pb/U isotopic ratios are calculated as zero ablation time intercepts of least-squares linear regression lines fitted to the time-resolved isotopic ratio data. This correction eliminates potential matrix differences between external standards and unknown samples because the intercept is calculated from the data for each individual sample. This method has been applied U-Pb LA-ICPMS dating of zircon (Košler et al., 2002), monazite (Košler et al., 2001) and perovskite (Cox and Wilton, 2006) and is well suited to target minerals, such as apatite, for which no matrix-matched standard exists.

The analytical uncertainty due to the elemental fractionation corrections increases with the size of the correction. It is therefore important to minimize fractionation, and various laser parameters can be used to suppress it. Laser-induced fractionation may also be limited by scanning the stage beneath the stationary laser beam. This produces a linear traverse or raster in the sample (Košler et al. 2002), and the effect is similar to drilling a large shallow laser pit, which produces only limited Pb/U fractionation (Eggins et al. 1998, Mank and Mason 1999).

3.3 Analytical procedure

Samples were mounted on 2.5 cm diameter epoxy disks and analysed using a Thermo ELEMENT XR double focusing magnetic sector field ICP-MS in combination with a Geolas 193 nm ArF Excimer laser located in the Inco Innovation Centre, Memorial University of Newfoundland, Canada. Samples were ablated using a 10 μm laser beam that was rastered over the sample surface to create a 40 × 40 μm square to minimize laser-induced Pb/U fractionation. A small subset of analyses employed a 60 × 60 μm square using a 20μm laser beam. The laser energy was set at 3 J/cm^2 with a repetition rate of 10 Hz. The ablated apatite material was flushed from the sample cell with a helium carrier gas and combined with argon gas before entering the plasma source of the mass spectrometer. A T-piece tube attached to the back end of the plasma torch enabled simultaneous nebulization of an internal standard tracer solution consisting of a mixture of natural Tl (^{205}Tl/^{203}Tl = 2.3871) and enriched ^{233}U, ^{209}Bi and ^{237}Np (concentrations of ca. 1 ppb per isotope) which was used to correct for instrumental mass bias (Figure 1). The isotopic ratios in the tracer solution have a mean isotopic mass similar to that of the isotopic ratios being corrected in the analyzed apatites and the tracer isotopes also have ionization potentials and rates of oxide formation in the ICPMS which are similar to the isotopes of interest in the apatite sample (cf. Hirata 1996). The tracer solution approach to monitoring mass bias is preferred to analysing the equivalent isotopic ratios (e.g., ^{205}Tl/^{203}Tl) in NIST SRM 610 standard glass because it facilitates monitoring of the mass bias at all times. For example, if the machine mass bias drifts or changes due to matrix effects of a particular ablation it can be observed when analysing both standards and unknowns. In dry plasma or bracketing mode it is assumed the mass bias stays constant between analyses of the NIST SRM 610 glasses which is not always the case.

Data were collected in peak-jumping mode, using 1 point per mass peak with a 60 s gas blank and a 180 s signal. Measured masses were: ^{200}Hg, ^{202}Hg, ^{203}Tl, ^{204}Hg+Pb, ^{205}Tl, ^{206}Pb, ^{207}Pb, ^{208}Pb, ^{209}Bi, ^{232}Th ^{233}U, ^{237}Np, ^{238}U and oxide masses of 248 (^{232}Th^{16}O), 249 (^{233}U^{16}O), 253 (^{237}Np^{16}O) and 254 (^{238}U^{16}O). The natural ^{238}U/^{235}U ratio of 137.88 was used to calculate ^{235}U. The level of oxide production is less than 0.5% for dry analyses, but is ca. 3% for NpO, 5% for UO and 15% for ThO during aspiration of the tracer solution. Raw data were processed off-line using an Excel spreadsheet program (LAMDATE) to integrate signals from each sequential set of 10 sweeps. The spreadsheet corrects for U–Pb, Th-Pb and Th-U fractionation due to volatility differences during laser ablation by using the back-calculated intercept of

the time resolved signal (already corrected for mass bias) (Figure 1) following the method described in Košler et al. (2002). $^{207}Pb/^{206}Pb$, $^{208}Pb/^{206}Pb$, $^{206}Pb/^{238}U$, $^{207}Pb/^{235}U$, $^{208}Pb/^{232}Th$ and $^{232}Th/^{238}U$ ratios were calculated and blank corrected for each analysis.

Several external standards were analysed after every five analyses of apatite unknowns as a quality control to monitor variability and drift in operating conditions during a session. $^{207}Pb/^{206}Pb$ (and hence also $^{208}Pb/^{206}Pb$) and $^{206}Pb/^{238}U$ ratios were monitored by analysis of two zircon standards: 337.13 ± 0.37 Ma Plešovice zircon (Sláma et al., 2008) and ca. 1065 Ma Harvard 91500 zircon (Wiedenbeck et al., 1995) whose U-Pb and $^{207}Pb/^{206}Pb$ ages have previously been determined by ID-TIMS. $^{207}Pb/^{206}Pb$ (and also $^{208}Pb/^{206}Pb$) ratios were also monitored by analysis of the STDP5 phosphate glass (Klemme et al., 2008) which yields a value of 0.8572 ± 0.0020 (2σ) in this study. $^{208}Pb/^{232}Th$ ratios were monitored by analysis of Plešovice zircon (Sláma et al., 2008) and 91500 zircon which yields a $^{208}Pb/^{232}Th$ age of 1062.1 ± 2.2 Ma (Amelin and Zaitsev, 2002). $^{206}Pb/^{238}U$, $^{207}Pb/^{206}Pb$, and $^{208}Pb/^{232}Th$ ages for Plešovice zircon are 337.7 ± 4.0 Ma, 329.1 ± 9.3 Ma and 327 ± 10 Ma (2σ, n = 29) and 1076 ± 26 Ma, 1068 ± 15 Ma and 1070 ± 65 Ma for 91500 zircon (2σ, n = 6) respectively. $^{232}Th/^{238}U$ ratios were monitored by analysing NIST SRM 610 standard glass which has a mean TIMS Th/U ratio of 0.9866 ± 0.0018 (Stern and Amelin, 2003), which corresponds to a $^{232}Th/^{238}U$ ratio of 1.0136 ± 0.0018 using the $^{238}U/^{235}U$ abundance ratios of 417.8 in NIST SRM 610 standard glass (Stern and Amelin, 2003). This is within analytical uncertainty of the value of 1.0156 ± 0.0051 (2σ, n = 36) reported in this study. NIST SRM 610 standard glass cannot be used in this study to monitor any Pb isotopic ratio as it contains Bi and Tl which interferes with the solution-based mass bias correction.

Isotopic ratios and uncertainties on individual analyses are reported with 2σ errors in Table 2. Error ellipses on the individual analyses on the Tera-Wasserburg Concordia (Figure 2) are displayed at the 1σ level for clarity, while error bars on the weighted average ages in Figure 2 are at the 2σ level. Tera-Wasserburg Concordia ages, Tera-Wasserburg Concordia ages anchored through common Pb, and weighted average ^{207}Pb-corrected and ^{208}Pb-corrected ages are all reported with 2σ errors in Table 3 and on Figure 2. Representative Th, U and Pb concentrations for each apatite sample were calibrated against NIST SRM 610 standard glass and are listed in Table 3. Although glass is not an ideal concentration standard as it is not matrix matched to

apatite, the data serve as a useful approximation for the absolute element concentrations of the apatite samples. Relative elemental concentration ratios between the apatite samples are also independent of this standard glass calibration.

4. Results

Age calculations employed between 11 and 33 analyses per sample (Fig. 2, Table 2). Of the four separate approaches for common Pb correction, the weighted average of the ^{207}Pb-corrected ages and the Tera-Wasserburg Concordia intercept age anchored through common Pb are very similar (Table 3). This is not surprising given that a ^{207}Pb-corrected age is a projection through common Pb onto the ^{238}U/^{206}Pb axis of the Tera-Wasserburg Concordia. Hence the ^{207}Pb-corrected ages and the anchored Tera-Wasserburg Concordia intercept ages will be considered together.

2σ weighted-mean age uncertainties on the ^{207}Pb-corrected ages range from 1.2% - 8.8%, which are very similar to the uncertainties on the Tera-Wasserburg Concordia intercept ages (1.3% – 8.5%). The samples with the greatest age uncertainties are either U-poor samples (Mudtank apatite with 8.96 ppm U and a 8.8% 2σ uncertainty on the weighted average ^{207}Pb-corrected age and DC 4/5/2 apatite with 9.89 ppm U and a 7.6% 2σ uncertainty on the weighted average ^{207}Pb-corrected age) or young (the 31.44 ± 0.18 Ma Durango apatite with a 7.6% 2σ uncertainty on the weighted average ^{207}Pb-corrected age. Two of the weighted average ^{207}Pb-corrected ages and anchored Tera-Wasserburg lower intercept ages fall just outside the uncertainty limits on the assumed age of the reference material (Table 3). These are the ca. 460 Ma Slyudyanka apatite (TW anchored Concordia age of 448 ± 7.3 Ma, Fig. 2Y; ^{207}Pb-corrected age of 447 ± 7.3 Ma, Fig. 2a) and the ca. 395 Ma granitoid sample, DC 4/5/2 (TW anchored Concordia age of 364 ± 21 Ma, Fig. 2c; ^{207}Pb-corrected age of 361 ± 27 Ma, Fig. 2e). Additionally the assumed age of Otter Lake apatite (913 ± 7 Ma) is 1 Ma outside the uncertainty limit on the TW anchored Concordia age of 933 ± 12 Ma, Fig. 2U), although the possibility remains that that the assumed Pb-Pb age is discordant.

In contrast, the unanchored Tera-Wasserburg Concordia intercept ages yield by far the most imprecise age data, with 2σ uncertainties ranging between 11 and 64% (Table 3). Five of the eight ages are within 2σ uncertainty of the adopted reference ages (Table 1), with Mineville (Fig. 2N, 883 ± 98 Ma, reference age 990 – 1040 Ma),

Emerald Lake (Fig. 2X, 260 ± 150 Ma, reference age 92.2 Ma) and Mudtank (Fig. 2R, 1163 ± 750 Ma, reference age 349 Ma) not overlapping with the adopted age of the reference material. The uncertainty on the unanchored Tera-Wasserburg Concordia intercept ages is a function of the data spread on the Tera-Wasserburg Concordia. Assuming that all the $^{238}U/^{206}Pb^*$ ages overlap within analytical uncertainty, then there needs to be both a large spread in common Pb / radiogenic Pb ratios and for some analyses to contain low amounts of common Pb in order to define a well constrained linear array on the Concordia. The samples with the highest uncertainties (Emerald Lake with a 2σ uncertainty of 58% and Mudtank with a 2σ uncertainty of 64%, Table 3) have error ellipses which cluster closely together on the Tera-Wasserburg Concordia, and in the case of Mudtank apatite, also contain significant proportions of common Pb.

The weighted average ^{208}Pb-corrected ages yield the most variable data with 2σ uncertainties ranging between 0.8 and 81% (Table 3). Ages denoted with an asterisk in Table 3 are uncorrected $^{208}Pb/^{232}Th$ ages. A ^{208}Pb-correction cannot be applied to these high Th/U samples (the Durango, Kovdor, Mineville and Otter Lake apatites) as the ^{208}Pb correction becomes inappropriate as the $^{232}Th/^{238}U$ ratio approaches 7 (see Appendix A). However, these samples are characterised by high Th concentrations and high radiogenic ^{208}Pb to common ^{208}Pb ratios (Table 2) and so uncorrected $^{208}Pb/^{232}Th$ ages are presented instead. Even so, these $^{208}Pb/^{232}Th$ ages still contain some common Pb and therefore represent maximum age constraints. Analytical uncertainties on the $^{208}Pb/^{232}Th$ ages of these high Th samples are low, even for the 31.44 Ma Durango apatite which yields an uncorrected $^{208}Pb/^{232}Th$ age of 32.5 ± 1.2 Ma (2σ uncertainty of 3.7%, Fig. 2D). Analytical uncertainties are greatest on low Th, high Th/U samples such as Mudtank apatite. This yields a weighted average ^{208}Pb-corrected age of 459 ± 370 Ma (2σ uncertainty of 81%) with a low Th concentration of 47.3 ppm and a Th/U ratio of 5.27 (Table 3). In contrast, even though it has a much lower Th concentration (7.28 ppm) and is of similar age to Mudtank apatite, the uncertainty on the granitoid sample DC 4/5/2 is much lower (2σ uncertainty of 24% on an age of 390 ± 92 Ma) due to the low Th/U ratio of 0.74. Two of the Th-Pb ages fall marginally outside the uncertainty limits on the assumed age of the reference material (Table 3). These are the ca. 92.2 Ma Emerald Lake apatite (weighted average ^{208}Pb-corrected age of 105.0 ± 9.0 Ma, Fig. 2H) and the 913 ± 7 Ma Otter Lake apatite (weighted average $^{208}Pb/^{232}Th$ age of 941 ± 8.5 Ma, Fig. 2X).

5. Discussion

The samples yield U-Pb and Th-Pb ages which are in general consistent with independent estimates of the U-Pb apatite age, which demonstrates the suitability of the both analytical protocol and the correction methods (for common Pb and laser-induced Pb / U fractionation) employed. Laser-induced Pb / U fractionation was relatively minor (typically less than ± 5%), and was easily corrected for using the back-calculated intercept of the time resolved signal (Figure 1). In an attempt to monitor the effect of laser-spot size and analyte volume on the final age precision, a subset of analyses of two reference materials (Durango and Emerald Lake apatite, Fig. 2C and Fig. 2G) was undertaken by rastering a 20μm laser beam over a 60 x 60μm square. This resulted in a four-fold increase in signal intensity and a slight increase in laser-induced Pb / U fractionation, but did not result in a significant improvement in the precision on the isotopic ratios. For the Durango sample, the average precision on $^{206}Pb/^{238}U$ ratios actually decreased from 17.1% to 17.4% and the average precision on $^{207}Pb/^{206}Pb$ ratios decreased from 8.1% to 10.8%. In contrast, for the Emerald Lake sample, the average precision on $^{206}Pb/^{238}U$ ratios increased from 9.4% to 6.7% and on $^{207}Pb/^{206}Pb$ ratios from 3.6% to 2.4% when using the 60 x 60μm raster.

5.1 Common Pb correction and implications for provenance analysis

As one of the main applications of U-Th-Pb apatite dating by ICPMS is likely to be detrital apatite dating in sedimentary provenance studies, it is important that the common Pb correction employed is applicable to single apatite grains. The spread in U / total Pb ratios in the apatite samples of this study in general do not yield precise unanchored Tera-Wasserburg Concordia intercept ages. For example, the granodiorite sample (DC 4/5/2), which would be a typical source of sand-sized detrital apatite grains, did not yield a large spread in U / total Pb ratios and thus has a large 2σ uncertainty on the unanchored Tera-Wasserburg Concordia age (2σ uncertainty of 28%, Table 3, Fig. 2d). The ^{207}Pb- and ^{208}Pb-correction methods used in conjunction with the Stacey and Kramers (1975) model for crustal Pb evolution would appear to be the most applicable for single grain detrital apatite dating, as the intercept age-based approaches using the Tera-Wasserburg Concordia would require multiple

analyses on the same detrital grain which is unlikely to yield a sufficient spread in the common Pb / radiogenic Pb ratio. Obtaining both U-Pb and Th-Pb ages also has the added advantage of yielding two separate age constraints for the same grain. In samples which have high Th concentrations, high Th/U ratios (> 5) and low f_{208} values, the uncorrected $^{208}Pb/^{232}Th$ age may be preferred to the ^{208}Pb-corrected age.

However, Pb correction using the Stacey and Kramers (1975) model does require an initial assumption of the age of the grain, which is not typically known for a suite of grains in a detrital sample. However, it can be approximated successfully using an iterative approach combined with the Stacey and Kramers (1975) model. The approach involves calculating a ^{207}Pb-corrected age (or equally a ^{208}Pb-corrected age) using a Pb isotopic composition calculated with the Stacey and Kramers (1975) model for an initial age estimate of 1 Ga. This ^{207}Pb-corrected age is then used to calculate a new Pb isotopic composition using the Stacey and Kramers (1975) model, and an updated ^{207}Pb-corrected age is calculated. This iterative approach is repeated five times, by which stage the change in the ^{207}Pb-corrected age between iterations is negligible. The final ^{207}Pb-corrected age differs by < 0.05% if an initial age estimate of 1 Ma is used instead of 1 Ga, demonstrating it is not dependent on the choice of initial age.

This approach is demonstrated using sample DC 4/5/2 as a case study, for which there are robust independent constraints on the initial Pb isotopic composition derived from K-feldspar analyses (Table 1, 3). Table 4 lists the ^{207}Pb- and ^{208}Pb-corrected ages employing an initial Pb isotopic composition based on the K-feldspar analyses and compares them with the data derived from the iterative approach outlined above. The weighted means of the ^{207}Pb- and ^{208}Pb-corrected ages which employ a Pb isotopic composition derived from K-feldspar analyses are 361 ± 27 Ma and 390 ± 92 Ma respectively (Table 4). The weighted means of the ^{207}Pb- and ^{208}Pb-corrected ages using the iterative approach are 366 ± 27 Ma and 394 ± 92 Ma, which represent a difference of 1.4% and 1% respectively (Table 4), demonstrating the suitability of the iterative approach for calculating an appropriate initial Pb isotopic composition for single detrital grains. It should be noted that the assumption that the initial Pb isotopic composition derived from the Stacey and Kramers (1975) model is correct may not always be appropriate, and that this assumption cannot be verified in samples where there is no independent control on the initial Pb isotopic composition such as detrital samples.

U-Th-Pb apatite dating by ICPMS has potential to be combined with other analytical methods for provenance work. Analytical techniques that could in principle be undertaken in conjunction with U-Th-Pb dating include fission track, (U-Th)/He or Nd isotopic analysis. Combining U-Th-Pb dating with either the apatite fission track or apatite (U-Th)/He thermochronometers would yield two pieces of information from the same grain – the age of formation of the apatite (using the U-Pb method), and the time the grains passed through the low temperature window for the retention of either fission tracks or radiogenic ^{4}He. Combining apatite U-Th-Pb dating with the apatite fission track method has an additional advantage. Fission track dating requires precise measurements of ^{238}U, which are conventionally determined by irradiating the sample with thermal neutrons in a nuclear reactor to induce fission in a proportion of ^{235}U atoms. These induced fission events are then recorded in an external detector (typically low U muscovite) to give a map of uranium distribution (Gleadow, 1981). This irradiation step is one of the disadvantages of the external detector method. However U concentrations in apatite fission track dating can also be determined by LA-ICPMS (Hasebe et al., 2004) with ^{44}Ca typically used as an internal standard. Although modification of the analytical protocol to include a peak jump to ^{44}Ca would be prohibitively slow on a magnetic sector instrument such as the one used in this study, U concentrations could be easily determined on a spot adjacent to the site of the U-Th-Pb analysis. Combining U-Th-Pb apatite dating by LA-ICPMS with the apatite (U-Th)/He thermochronometer is slightly more challenging as (U-Th)/He dating is performed on whole crystals, not polished grain mounts. However several studies have undertaken U-Pb detrital zircon dating by LA-ICPMS on the exterior of unmodified zircon grains (e.g., Rahl et al., 2003), and modifying this procedure for apatite double dating is entirely possible. Combining U-Th-Pb apatite dating with Nd isotopic analysis (e.g., Foster and Vance, 2006) is also feasible. This would yield similar information to combined U-Pb and Hf isotopic studies on zircon, with the U-Th-Pb age data and the Nd isotopes yielding information concerning the apatite crystallization age and melt source respectively.

5.2 Effect of excess ^{206}Pb on age calculations

U-Pb dating of minerals characterized by high Th/U ratios (e.g., Durango and Kovdor Carbonatite apatite in this study) can be affected by excess ^{206}Pb derived from

^{230}Th, an intermediate daughter nuclide of the ^{238}U decay series incorporated in excess of its secular equilibrium ratio (Schärer, 1984). This results in apparent ^{206}Pb/^{238}U ages which are older than the corresponding ^{207}Pb/^{235}U and ^{208}Pb/^{232}Th ages from the same sample, and is a particularly important effect in young minerals where the excess ^{206}Pb is not diluted by radiogenic ^{206}Pb. In high-precision TIMS studies of monzatite this effect can be accounted for by evaluating the concordance of ^{206}Pb/^{238}U, ^{207}Pb/^{235}U and ^{208}Pb/^{232}Th ages. With more imprecise LA-ICPMS data, the effect of ^{230}Th disequilibrium in high Th/U samples (particularly apatite which requires a substantial common Pb correction) is more difficult to evaluate without independent constraints on the magma Th/U ratio.

The effect of ^{230}Th disequilibrium is most pronounced when apatite with a high Th/U ratio crystallises from a melt with a low Th/U ratio. However, partition coefficients for U and Th in apatite crystallising from silicate melts are close to unity, and are not significantly affected by variations in magma compositions such as increasing SiO_2-content of the melt (Prowatke and Klemme, 2006). Hence ^{230}Th disequilibrium in apatite is unlikely to be a major factor in most silicate melts. U, Th are compatible in apatite crystallising from a carbonatite melt with D_{Th} apatite / carbonatite > 5 and D_U apatite / carbonatite ~ 2 (Hammouda et al., in press), and therefore it is possible to crystallise high Th/U apatite from carbonatitic liquids with a relatively low Th/U ratio. Despite the high Th/U of Kovdor Carbonatite apatite, it appears to have crystallized from a magma with Th/U ratios between 2 and 4 with uranium-series isotopes in the magma in secular equilibrium (Amelin and Zaitsev, 2002). All three decay schemes (^{206}Pb/^{238}U, ^{207}Pb/^{235}U and ^{208}Pb/^{232}Th) yield compatible TIMS ages with a small difference in ^{206}Pb/^{238}U *vs* ^{207}Pb/^{235}U age due to an excess of unsupported ^{206}Pb of about 1.5 Ma (or 0.4% of the age) (Amelin and Zaitsev, 2002). Such an age correction is insignificant when dealing with the level of precision routinely achieved through LA-ICPMS analysis of apatite.

5.3 A matrix-matched apatite standard for LA-ICPMS dating

An ideal matrix-matched apatite standard for LA-ICPMS dating would contain no common Pb, would have high U, Th and radiogenic Pb concentrations and would yield precise U-Pb and Th-Pb ages determined by TIMS. Currently, no such standard exists. Of the samples analysed in this study, the Kovdor carbonatite apatite exhibits

the most promise as an apatite standard for LA-ICPMS dating. It has high Th (3539 ppm), U (55.7 ppm) and Pb (65.0 ppm) concentrations, and the initial Pb isotopic composition is known (Amelin and Zaitsev, 2002). It should be noted that the Th and U concentrations reported here are significantly higher than those reported by Amelin and Zaitsev (2002), and so apatite samples from the Kovdor massif are variable in composition. Kovdor carbonatite apatite yields precise and reproducible ^{207}Pb-corrected, ^{232}Th-^{208}Pb, and common Pb-anchored Tera-Wasserburg Concordia intercept ages (Figs. 1I – 1L), with low precision on the ^{232}Th-^{208}Pb age (0.8% 2σ, Table 3).

6. Conclusions

This study has determined U-Pb and Th-Pb ages for seven well known apatite occurrences (Durango, Emerald Lake, Kovdor, Mineville, Mudtank, Otter Lake and Slyudyanka) and one unknown by LA-ICPMS. Analytical procedures typically involved rastering a 10μm spot over a 40×40μm square to a depth of 10μm using a Geolas 193nm ArF excimer laser coupled to a Thermo ElementXR single-collector ICPMS. All samples yield U-Pb and Th-Pb ages which are in general consistent with independent estimates of the U-Pb apatite age, which demonstrates the suitability of the both analytical protocol and the correction methods (for common Pb and laser-induced Pb / U fractionation) employed. In general, laser-induced Pb / U fractionation was relatively minor, and was easily corrected for using the back-calculated intercept of the time resolved signal. Age uncertainties are as low as 1-2% for Palaeozoic-Neoproterozoic samples with the uncertainty on the youngest sample, the Cenozoic (31.44 Ma) Durango apatite, ranging from 3.7–7.6% according to the common Pb-correction method employed.

Common Pb correction employed four separate approaches including the ^{207}Pb- and ^{208}Pb-correction methods, a Tera–Wasserburg Concordia and a Tera–Wasserburg Concordia anchored through common Pb. The common Pb composition for the anchored Tera–Wasserburg Concordia and the ^{207}Pb- and ^{208}Pb-correction methods employed either the initial Pb isotopic composition where known, or used the Stacey and Kramers (1975) model for crustal Pb evolution. Common Pb correction using the Stacey and Kramers model calculated the initial Pb isotopic composition using either the estimated age of the sample or an iterative approach. The age

difference between these two methods is typically less than 2%, suggesting that the iterative approach works well for samples where there are no constraints on the initial Pb composition, such as detrital samples. The unanchored Tera-Wasserburg Concordia ages typically did not yield a large spread in U / total Pb ratios and thus have large uncertainties. The ^{207}Pb- and ^{208}Pb-correction methods yielded more precise and accurate ages and would also appear to be the most suitable for single grain detrital apatite dating. In samples which have high Th concentrations, high Th/U ratios (> 5) and low f_{208} values, the uncorrected ^{208}Pb/^{232}Th age may be preferred to the ^{208}Pb-corrected age.

The accurate and relatively precise common Pb-corrected ages demonstrate the U-Pb and Th-Pb apatite chronometers are suitable as sedimentary provenance tools. The Kovdor carbonatite apatite is recommended as a potential U-Pb and Th-Pb apatite standard for LA-ICPMS analyses as the initial Pb isotopic composition is known, it has high Th, U and Pb concentrations and it yields precise and reproducible ^{207}Pb-corrected, ^{232}Th-^{208}Pb, and common Pb-anchored Tera-Wasserburg Concordia intercept ages.

Acknowledgements

This study was funded by the Ireland – Newfoundland Partnership and we gratefully acknowledge their financial support. John Hanchar is thanked for providing the Kovdor carbonatite, Mineville, Mudtank and Slyudyanka apatite samples. Courtney Gregory, an anonymous reviewer and editor Roberta Rudnick are thanked for extremely detailed reviews and suggestions which significantly improved this manuscript.

Appendix A. Mathematical correction approaches for common Pb

The ^{204}Pb-correction method

This method is based on the measurement of the low abundance non-radiogenic ^{204}Pb isotope. Measured Pb isotopic signals are corrected using the assumed ^{206}Pb/^{204}Pb, ^{207}Pb/^{204}Pb and ^{208}Pb/^{204}Pb ratios of the common Pb to extract net signal intensities of the radiogenic daughter ^{206}Pb*, ^{207}Pb*and ^{208}Pb* isotopes. A common notation for common Pb corrections is to define f_{206} as the fraction of total ^{206}Pb ($^{206}Pb_{total}$) that is common ^{206}Pb ($^{206}Pb_{common}$), such that:

$f_{206} = {}^{206}Pb_{common} / {}^{206}Pb_{total}$ Eq. (A.1)

It is then possible to calculate f_{206} from the assumed $^{206}Pb/^{204}Pb$ ratio for common Pb ($^{206}Pb/^{204}Pb_{common}$) and the measured $^{206}Pb/^{204}Pb$ ratio ($^{206}Pb/^{204}Pb_{measured}$) from:

$f_{206} = (^{206}Pb/^{204}Pb_{common}) / (^{206}Pb/^{204}Pb_{measured})$ Eq. (A.2)

Radiogenic $^{206}Pb/^{238}U$ ($^{206}Pb^*/^{238}U$) can then be calculated from the measured $^{206}Pb/^{238}U$ ($^{206}Pb/^{238}U_{measured}$) by:

$^{206}Pb^*/^{238}U = (1 - f) (^{206}Pb/^{238}U_{measured})$ Eq. (A.3)

The ^{208}Pb-correction method

This method is based on the assumption that the ratio of ^{232}Th to the parent U isotope in the analyzed sample has not been disturbed following the closure of the U-Pb and Th-Pb isotopic systems (i.e., the U-Th-Pb system is assumed to be concordant) and that any excess ^{208}Pb (e.g., $^{208}Pb_{measured}$ - $^{208}Pb^*$) can be attributed to the assumed common Pb component. The proportion of common ^{206}Pb in this case can be calculated as

$f_{206} = (^{208}Pb/^{206}Pb_{measured} - {}^{208}Pb^*/^{206}Pb^*) / (^{208}Pb/^{206}Pb_{common} - {}^{208}Pb^*/^{206}Pb^*)$ Eq. (A.4)

where the expected radiogenic $^{208}Pb^*/^{206*}Pb$ ratio can be calculated from the $^{232}Th/^{238}U$ ratio of the sample and estimated age (t) by:

$^{208}Pb^*/^{206}Pb^* = (^{232}Th / {}^{238}U) [(e^{\lambda_{232}t} - 1) / (e^{\lambda_{238}t} - 1)]$ Eq. (A.5)

and is relatively insensitive to small errors in t (Williams, 1998). This formulation works particularly well for targets with very low $^{232}Th/^{238}U$ (<0.5), but is not suitable for high Th/U targets (e.g. monazite, or the Durango, Kovdor, Mineville and Otter Lake apatites in this study), especially those where $^{232}Th/^{238}U$ approaches 7, in which case the $^{208}Pb^*/^{206}Pb^*$ ratio approaches the $^{208}Pb/^{206}Pb_{common}$ ratio (Williams, 1998).

Similar to Eq. (A.1), the fraction (f_{208}) of total ^{208}Pb ($^{208}Pb_{total}$) that is common ^{208}Pb ($^{208}Pb_{common}$) is:

$$f_{208} = {}^{208}Pb_{common} / {}^{208}Pb_{total} \quad \text{Eq. (A.6)}$$

In single-collector ICPMS instruments where it is often difficult to measure the low abundance ^{204}Pb isotope directly, f_{208} can be estimated from the measured $^{208}Pb/^{206}Pb$ ratio ($^{208}Pb/^{206}Pb_{measured}$), the assumed $^{208}Pb/^{206}Pb$ ratio of common Pb ($^{208}Pb/^{206}Pb_{common}$) and the f_{206} ratio by:

$$f_{208} = f_{206} \, (^{208}Pb/^{206}Pb_{common}) / (^{208}Pb/^{206}Pb_{measured}) \quad \text{Eq. (A.7)}$$

The ^{207}Pb-correction method

This method utilizes the measured $^{207}Pb/^{206}Pb$ ratios to calculate the proportion of common ^{206}Pb as:

$$f_{206} = (^{207}Pb/^{206}Pb_{measured} - {}^{207}Pb^*/^{206}Pb^*) / (^{207}Pb/^{206}Pb_{common} - {}^{207}Pb^*/^{206}Pb^*) \quad \text{Eq. (A.8)}$$

Similar to the ^{208}Pb-correction method, this correction also assumes that the U-Pb data are concordant. This method is commonly used in ion micro-probe studies for young (Phanerozoic) samples where the need to estimate radiogenic $^{206}Pb/^{238}U$ as accurately as possible outweighs the need to evaluate data concordance.

References

Amelin, Y. and Zaitsev, A.N., 2002. Precise geochronology of phoscorites and carbonatites: The critical role of U-series disequilibrium in age interpretations. Geochimica et Cosmochimica Acta, 66(13): 2399-2419.

Barfod, G.H., Krogstad, E.J., Frei, R. and Albarede, F., 2005. Lu-Hf and PbSL geochronology of apatites from Proterozoic terranes: A first look at Lu-Hf isotopic closure in metamorphic apatite. Geochimica et Cosmochimica Acta, 69(7): 1847-1859.

Barfod, G.H., Otero, O. and Albarède, F., 2003. Phosphate Lu-Hf geochronology. Chemical Geology, 200(3-4): 241-253.

Belousova, E.A., Griffin, W.L., O'Reilly, S.Y., Fisher, N.I., 2002. Apatite as an indicator mineral for mineral exploration: trace-element compositions and their relationship to host rock type. Journal of Geochemical Exploration, 76(1): 45-69.

Bernet, M. and Spiegel, C., 2004. Introduction: detrital thermochronology. Geological Society of America Special Papers, 378: 1-6.

Black, L.P. and Gulson, B.L., 1978. The age of the Mud Tank carbonatite, Strangways Range, Northern Territory. Bureau of Mineral Resources Journal of Australian Geology and Geophysics, 3: 227–232.

Brandon, M.T., Roden-Tice, M.K., Garver, J.I., 1998. Late Cenozoic exhumation of the Cascadia accretionary wedge in the Olympic Mountains, northwest Washington State. Geological Society of America Bulletin, 110(8): 985-1009.

Carrapa, B., DeCelles, P.G., Reiners, P.W., Gehrels, G.E. and Sudo, M., 2009. Apatite triple dating and white mica $^{40}Ar/^{39}Ar$ thermochronology of syntectonic detritus in the Central Andes: A multiphase tectonothermal history. Geology, 37(5): 407-410.

Carter, A. and Foster, G.L., 2009. Improving constraints on apatite provenance: Nd measurement on fission-track-dated grains. In: F. Lisker, B. Ventura and U.A. Glasmacher (Editors), Thermochronological methods; from palaeotemperature constraints to landscape evolution models. Geological Society London Special Publications 324, pp. 57-72.

Chamberlain, K.R. and Bowring, S.A., 2000. Apatite-feldspar U-Pb thermochronometer: A reliable, mid-range (450 °C), diffusion-controlled system. Chemical Geology, 172(1-2): 173-200.

Cherniak, D.J., Lanford, W.A., Ryerson, F.J., 1991. Lead Diffusion in Apatite and Zircon Using Ion-Implantation and Rutherford Backscattering Techniques. Geochimica Et Cosmochimica Acta, 55(6): 1663-1673.

Chew, D.M. et al., 2007. U-Pb geochronologic evidence for the evolution of the Gondwanan margin of the north-central Andes. Geological Society of America Bulletin., 119(5/6): 697-711.

Chew, D.M., Schaltegger, U., Miškovic, A., Fontignie, D. and Frank, M., 2005. Deciphering the tectonic evolution of the Peruvian segment of the Gondwanan margin, 6th International Symposium on Andean Geodynamics (ISAG 2005, Barcelona), Extended Abstracts, pp. 166–169.

Cocherie, A., 2009. Common-Pb correction in laser U-Pb geochronology using MC-ICPMS and a multi-ion counting system. Geochimica et Cosmochimica Acta, 73(13): A233-A233.

Cocherie, A., Fanning, C.M., Jezequel, P. and Roberta, M., 2009. LA-MC-ICPMS and SHRIMP U-Pb dating of complex zircons from Quaternary tephras from the French Massif Central: Magma residence time and geochemical implications. Geochimica et Cosmochimica Acta, 73(4): 1095-1108.

Coulson, I.M. et al., 2002. Time-scales of assembly and thermal history of a composite felsic pluton: constraints from the Emerald Lake area, northern Canadian Cordillera, Yukon. Journal of Volcanology and Geothermal Research, 114(3-4): 331-356.

Cox, R.A. and Wilton, D.H.C., 2006. U-Pb dating of perovskite by LA-ICP-MS: An example from the Oka carbonatite, Quebec, Canada. Chemical Geology, 235(1-2): 21-32.

Dempster, T.J., Jolivet, M., Tubrett, M.N. and Braithwaite, C.J.R., 2003. Magmatic zoning in apatite: a monitor of porosity and permeability change in granites. Contributions to Mineralogy and Petrology, 145(5): 568-577.

Eggins, S.M., Kinsley, L.P.J. and Shelley, J.M.G., 1998. Deposition and element fractionation processes during atmospheric pressure laser sampling for analysis by ICP-MS. Applied Surface Science, 127: 278-286.

Farley, K.A., 2000. Helium diffusion from apatite: General behavior as illustrated by Durango fluorapatite. Journal of Geophysical Research, 105(B2): 2903-2914.

Foose, M.P. and McLelland, J.M., 1995. Proterozoic low-Ti iron-oxide deposits in New York and New Jersey - Relation to Fe-oxide (Cu-U-Au-rare earth element) deposits and tectonic implications. Geology, 23(7): 665-668.

Foster, G.L. and Vance, D., 2006. In situ Nd isotopic analysis of geological materials by laser ablation MC-ICP-MS. Journal of Analytical Atomic Spectrometry, 21(3): 288-296.

Gehrels, G.E., Valencia, V.A. and Ruiz, J., 2008. Enhanced precision, accuracy, efficiency, and spatial resolution of U-Pb ages by laser ablation-multicollector-inductively coupled plasma-mass spectrometry. Geochemistry Geophysics Geosystems, 9: 13pp.

Gibson, G.M. and Ireland, T.R., 1996. Extension of Delamerian (Ross) orogen into western New Zealand: Evidence from zircon ages and implications for crustal growth along the Pacific margin of Gondwana. Geology, 24(12): 1087-1090.

Gleadow, A.J.W., 1981. Fission-track dating methods: what are the real alternatives? Nuclear Tracks, 5(1-2): 3-14.

Green, P.F., Crowhurst, P.V., Duddy, I.R., Japsen, T. and Holford, S.P., 2006. Conflicting (U-Th)/He and fission track ages in apatite: Enhanced He retention, not anomalous annealing behaviour. Earth and Planetary Science Letters, 250(3-4): 407-427.

Gregory, C.J., McFarlane, C.R.M., Hermann, J., Rubatto, D., 2009. Tracing the evolution of calc-alkaline magmas: In-situ Sm-Nd isotope studies of accessory minerals in the Bergell Igneous Complex, Italy. Chemical Geology, 260(1-2): 73-86.

Gregory, C.J. et al., 2007. Allanite micro-geochronology: A LA-ICP-MS and SHRIMP U-Th-Pb study. Chemical Geology, 245(3-4): 162-182.

Haines, P.W., Hand, M. and Sandiford, M., 2001. Palaeozoic synorogenic sedimentation in central and northern Australia: a review of distribution and timing with implications for the evolution of intracontinental orogens. Australian Journal of Earth Sciences, 48(6): 911-928.

Hammouda, T., Chantel, J., Devidal, J-L., in press. Apatite solubility in carbonatitic liquids and trace element partitioning between apatite and carbonatite at high pressure. Geochimica et Cosmochimica Acta.

Hasebe, N., Barbarand, J., Jarvis, K., Carter, A. and Hurford, A.J., 2004. Apatite fission-track chronometry using laser ablation ICP-MS. Chemical Geology, 207(3-4): 135-145.

Hirata, T., 1996. Lead isotopic analyses of NIST standard reference materials using multiple collector inductively coupled plasma mass spectrometry coupled with a modified external correction method for mass discrimination effect. Analyst, 121(10): 1407-1411.

Horn, I., Rudnick, R.L. and McDonough, W.F., 2000. Precise elemental and isotope ratio determination by simultaneous solution nebulization and laser ablation-ICP-MS: application to U-Pb geochronology. Chemical Geology, 164(3-4): 281-301.

Jackson, S.E., Longerich, H.P., Horn, I. and Dunning, R., 1996. The application of laser ablation microprobe (LAM)-ICP-MS to in situ U–Pb zircon geochronology. Journal of Conference Abstracts, 1: 283.

Klemme, S. et al., 2008. Synthesis and preliminary characterisation of new silicate, phosphate and titanite reference glasses. Geostandards and Geoanalytical Research, 32(1): 39-54.

Košler, J., Fonneland, H., Sylvester, P., Tubrett, M. and Pedersen, R.B., 2002. U-Pb dating of detrital zircons for sediment provenance studies - a comparison of laser ablation ICPMS and SIMS techniques. Chemical Geology, 182(2-4): 605-618.

Košler, J. and Sylvester, P.J., 2003. Present trends and the future of zircon in geochronology: laser ablation ICPMS. Reviews in Mineralogy and Geochemistry, 53: 243-275.

Košler, J., Tubrett, M.N. and Sylvester, P.J., 2001. Application of laser ablation ICP-MS to U-Th-Pb dating of monazite. Geostandards Newsletter - the Journal of Geostandards and Geoanalysis, 25(2-3): 375-386.

Kramm, U., Kogarko, L.N., Kononova, V.A. and Vartiainen, H., 1993. The Kola Alkaline Province of the CIS and Finland - Precise Rb-Sr Ages define 380-360 Ma age range for all magmatism. Lithos, 30(1): 33-44.

Kretz, R., Campbell, J.L., Hoffman, E.L., Hartree, R. and Teesdale, W.J., 1999. Approaches to equilibrium in the distribution of trace elements among the principal minerals in a high-grade metamorphic terrane. Journal of Metamorphic Geology, 17(1): 41-59.

Laslett, G.M., Green, P.F., Duddy, I.R. and Gleadow, A.J.W., 1987. Thermal annealing of fission tracks in apatite. II: A quantitative analysis. Chemical Geology, 65(1): 1-3.

Ludwig, K.R., 1998. On the treatment of concordant uranium-lead ages. Geochimica et Cosmochimica Acta, 62(4): 665-676.

Lupulescu, M.V. and Pyle, J.M., 2005. The Fe P REE deposit at Mineville, Essex Co., NY: manifestations of Precambrian and Mesozoic fluid infiltration events, GSA Northeastern Section - 40th Annual Meeting (March 14–16, 2005) Geological Society of America Abstracts with Programs, 37, pp. 4.

Mamani, M., Tassara, A., Woerner, G., 2008. Composition and structural control of crustal domains in the central Andes. Geochemistry Geophysics Geosystems, 9: -.

Mank, A.J.G. and Mason, P.R.D., 1999. A critical assessment of laser ablation ICP-MS as an analytical tool for depth analysis in silica-based glass samples. Journal of Analytical Atomic Spectrometry, 14(8): 1143-1153.

McDowell, F.W., McIntosh, W.C. and Farley, K.A., 2005. A precise ^{40}Ar-^{39}Ar reference age for the Durango apatite (U-Th)/He and fission-track dating standard. Chemical Geology, 214(3-4): 249-263.

McLelland, J.M. and Foose, M.P., 1996. Proterozoic low-Ti iron-oxide deposits in New York and New Jersey: Relation to Fe-oxide (Cu-U-Au-rare earth element) deposits and tectonic implications: Reply. Geology, 24(5): 476-477.

Mezger, K., Rawnsley, C.M., Bohlen, S.R. and Hanson, G.N., 1991. U-Pb garnet, sphene, monazite, and rutile Ages - Implications for the duration of high-grade metamorphism and cooling histories, Adirondack Mountains, New York. Journal of Geology, 99(3): 415-428.

Morton, A.C. and Hallsworth, C.R., 1999. Processes controlling the composition of heavy mineral assemblages in sandstones. Sedimentary Geology, 124: 3-29.

Piccoli, P.M. and Candela, P.A., 2002. Apatite in igneous systems. Reviews in Mineralogy and Geochemistry, 48(1): 255.

Prowatke, S., Klemme, S., 2006. Trace element partitioning between apatite and silicate melts. Geochimica Et Cosmochimica Acta, 70(17): 4513-4527.

Rahl, R.M., Reiners, P.W., Campbell, I.H., Nicolescu, S. and Allen, C.M., 2003. Combined single-grain (U-Th)/He and U/Pb dating of detrital zircons from the Navajo Sandstone, Utah. Geology, 31(9): 761-764.

Reznitskii, L.Z., Fefelov, N.N., Vasil'ev, E.P., Zarudneva, N.V. and Nekrasova, E.A., 1998. Isotopic composition of lead from metaphosphorites and problem of the Slyudyanka Group age, the southern Baikal - Western Khamar Daban region. Lithology and Mineral Resources 33(5): 432-441.

Reznitskii, L.Z. et al., 2000. The age and time span of the origin of phlogopite and lazurite deposits in the southwestern Baikal area: U-Pb geochronology. Petrology, 8(1): 66-76.

Reznitskii, L.Z., Sandimirova, G.P., Pakhol'chenko, Y.A. and Kuznetsova, S.V., 1999. The Rb-Sr age of the phlogopite deposits in Slyudyanka, southern Baikal region. Doklady Earth Sciences, 367: 711-713.

Salnikova, E.B. et al., 1998. U-Pb zircon dating of granulite metamorphism in the Sludyanskiy Complex, eastern Siberia. Gondwana Research, 1(2): 195-205.

Schärer, U., 1984. The Effect of Initial ^{230}Th Disequilibrium on Young U-Pb Ages - the Makalu Case, Himalaya. Earth and Planetary Science Letters, 67(2): 191-204.

Schoene, B. and Bowring, S.A., 2007. Determining accurate temperature-time paths from U-Pb thermochronology: An example from the Kaapvaal craton, southern Africa. Geochimica et Cosmochimica Acta, 71(1): 165-185.

Simonetti, A., Heaman, L.M., Chacko, T. and Banerjee, N.R., 2006. In situ petrographic thin section U-Pb dating of zircon, monazite, and titanite using laser ablation-MC-ICP-MS. International Journal of Mass Spectrometry, 253(1-2): 87-97.

Slama, J. et al., 2008. Plešovice zircon – a new natural reference material for U-Pb and Hf isotopic microanalysis. Chemical Geology, 249(1-2): 1-35.

Spear, F.S. and Pyle, J.M., 2002. Apatite, monazite, and xenotime in metamorphic rocks. Reviews in Mineralogy and Geochemistry, 48(1): 293.

Stacey, J.S. and Kramers, J.D., 1975. Approximation of terrestrial lead isotope evolution by a two-stage model. Earth and Planetary Science Letters, 26(2): 207-221.

Stern, R.A. and Amelin, Y., 2003. Assessment of errors in SIMS zircon U-Pb geochronology using a natural zircon standard and NIST SRM 610 glass. Chemical Geology, 197(1-4): 111-142.

Storey, C.D., Smith, M.P. and Jeffries, T.E., 2006. In situ LA-ICP-MS U-Pb dating of metavolcanics of Norrbotten, Sweden: Records of extended geological histories in complex titanite grains. Chemical Geology, 240(1-2): 163-181.

Sylvester, P.J. and Ghaderi, M., 1997. Trace element analysis of scheelite by excimer laser ablation inductively coupled plasma mass spectrometry (ELA-ICP-MS) using a synthetic silicate glass standard. Chemical Geology, 141(1-2): 49-65.

Tyrrell, S., Haughton, P.D.W., Daly, J.S., 2007. Drainage re-organization during break-up of Pangea revealed by *in-situ* Pb isotopic analysis of detrital K-feldspar. Geology, 35: 971-974.

Whitney, P.R., 1996. Proterozoic low-Ti iron oxide deposits in New York and New Jersey: Relation to Fe-oxide (Cu-U-Au-rare earth element) deposits and tectonic implications: Comment. Geology, 24(4): 382-383.

Whitney, P.R. and Olmsted, J.F., 1988. Geochemistry and origin of albite gneisses, northeastern Adirondack Mountains, New York. Contributions to Mineralogy and Petrology, 99(4): 476-484.

Wiedenbeck, M. et al., 1995. Three natural zircon standards for U-Th-Pb, Lu-Hf, trace element and REE analyses. Geostandards Newsletter, 19(1): 1-23.

Williams, I.S., 1998. U-Th-Pb geochronology by ion microprobe. In: McKibben, M.A., Shanks III, W.C., Ridley, W.I. (Eds.), Applications of microanalytical techniques to understanding mineralizing processes. Reviews in Economic Geology, (7): pp. 1–35.

Willigers, B.J.A., Baker, J.A., Krogstad, E.J. and Peate, D.W., 2002. Precise and accurate in situ Pb-Pb dating of apatite, monazite, and sphene by laser ablation multiple-collector ICP-MS. Geochimica et Cosmochimica Acta, 66(6): 1051-1066.

Figure captions

Figure 1 A). Time-resolved signal collected from a dry, single-spot ablation (40 μm) of Otter Lake apatite. R_0 is the intercept value calculated from regression of the fractionating $^{207}Pb/^{235}U$ data. The $^{232}Th/^{238}U$ signal exhibits significantly less fractionation than the $^{207}Pb/^{235}U$ or $^{206}Pb/^{238}U$ ratios. B) Non-fractionating, time-resolved signal collected from laser raster ablation (40 μm × 40 μm raster with a 10 μm spot) of Otter Lake apatite with simultaneous nebulization of tracer solution containing ^{205}Tl, ^{209}Bi, ^{233}U and ^{237}Np. The tracer solution ratios are represented by dashed lines and the tracer solution is continually aspirated during the analysis session.

Figure 2 (A-Z, a-f). Tera-Wasserburg Concordia diagrams anchored through common Pb (left column), unanchored Tera-Wasserburg Concordia diagrams (second column from the left), weighted average ^{207}Pb-corrected ages (second column from the right) and weighted average (either ^{208}Pb-corrected or $^{208}Pb/^{232}Th$) ages (right column) for the apatite samples dated in this study.

Table 1

Table 1
Summary of apatite age constraints from the literature

Apatite Standard	Age ± 2σ (Ma)	Method	Reference	common $^{208}Pb/^{206}Pb$, $^{207}Pb/^{206}Pb$†	Adopted age
Durango	31.44 ± 0.18 Ma	$^{40}Ar/^{39}Ar$, weighted mean of four single crystal sanidine-anorthoclase analyses	McDowell et al. (2005)	2.06793, 0.83771: SK(0.03)	31.44 ± 0.18 Ma
	31.02 ± 2.02 Ma	weighted mean (U-Th)/He age of 24 analyses	McDowell et al. (2005)		
Emerald Lake	94.5 - 92.2 Ma	^{40}Ar-^{39}Ar and U-Pb geochronology	Coulson et al. (2002)	2.07250, 0.84186: SK (0.094)	92.2 ± 0.9 Ma
	94.5 ± 0.2 Ma	U-Pb zircon, one fraction concordant	Coulson et al. (2002)		
	93.8 ± 1.4 Ma	U-Pb titanite, one fraction concordant	Coulson et al. (2002)		
	92.8 ± 0.2 Ma	U-Pb zircon, one fraction concordant	Coulson et al. (2002)		
	92.2 ± 0.9 Ma	U-Pb titanite, one fraction concordant	Coulson et al. (2002)		
	93.6 ± 0.7 Ma	$^{40}Ar/^{39}Ar$ hornblende	Coulson et al. (2002)		
	93.4 ± 0.7 Ma	$^{40}Ar/^{39}Ar$ biotite	Coulson et al. (2002)		
	93.5 ± 0.7 Ma	$^{40}Ar/^{39}Ar$ hornblende, hint of excess argon	Coulson et al. (2002)		
	93.7 ± 0.7 Ma	$^{40}Ar/^{39}Ar$ biotite, mildly disturbed	Coulson et al. (2002)		
	93.1 ± 0.7 Ma	$^{40}Ar/^{39}Ar$ biotite	Coulson et al. (2002)		
Kovdor carbonatite	376.4 ± 0.6 Ma	Weighted mean of four $^{208}Pb/^{232}Th$ apatite ages	Amelin and Zaitsev (2002)	2.05591, 0.83087: low U calcite	377.5 ± 3.5 Ma
	377.5 ± 3.5Ma	Total Pb/U apatite isochron	Amelin and Zaitsev (2002)		
	380.6 ± 2.6 Ma	Total Pb/U apatite - calcite isochron	Amelin and Zaitsev (2002)		
Mineville	1070 - 1050 Ma	Pre-ore (magnetite, hematie, apatite) regional crustal melting	Foose and McLelland (1995)	2.15856, 0.91219: SK(1.04)	1040 – 990 Ma
	1048 - 1035 Ma	Late-post tectonic igneous rocks, broadly contemporanous with ore bodies	McLelland and Foose (1996)		
	1030 - 990 Ma	Late metamorphic U/Pb garnet and sphene ages	Mezger et al. (1991)		
Mud Tank	735 ± 75 Ma	Rb-Sr whole rock	Black and Gulson (1978)	2.09885, 0.86485: SK(0.43)	ca. 349 Ma
	732 ± 5 Ma	U-Pb zircon	Black and Gulson (1978)		
	319 - 349 Ma	Rb-Sr Biotite ages, reset during Alice Springs Orogeny	Haines et al. (2001)		
	298 ± 23 Ma	Apatite fission track age	Green et al. (2006)		
Otter Lake, Yates Mine	913 ± 7 Ma	$^{207}Pb/^{206}Pb$ apatite stepwise leaching	Barfod et al. (2005)	2.14650, 0.90309: SK(0.93)	913 ± 7 Ma
Slyudyanka	465 ± 3 Ma	Apatite - whole rock Pb-Pb isochron	Reznitskii (1998)	2.09885, 0.86485: SK(0.43)	ca. 460 Ma
	456 ± 18 Ma	Apatite - whole rock Pb-Pb isochron	Reznitskii (1998)		
	460 ± 7 Ma	Rb-Sr phlogopite-calcite-apatite isochron	Reznitskii et al. (1999)		
	471 ± 2 Ma	U-Pb zircon age of an early syenite	Salnikova et al. (1998)		
	447 ± 2 Ma	U-Pb zircon age of a post-phlogopite assemblage pegmatite	Reznitskii et al. (2000)		
DC 4/5/2	442.4 ± 1.4 Ma	U-Pb zircon TIMS Concordia age	Chew et al. (2007)	2.089 ± 0.023, 0.857 ± 0.008*	394.6 ± 2 Ma
	444.2 ± 6.4 Ma	U-Pb zircon LA-ICPMS Concordia age	Chew et al. (2007)		
	394.6 ± 2 Ma	$^{40}Ar/^{39}Ar$ biotite	Chew unpublished data		

†initial Pb compostions are those used for used for common Pb correction in this study. They employ the Stacey and Kramers (1975) Pb evolution model (for an age in Ga) unless otherwise stated. *LA-MC-ICPMS analyses of K-feldspar undertaken in Memorial University during the course of this study

Table 2
Apatite isotopic and age data

	$^{207}Pb/^{235}U$	± 2σ	$^{206}Pb/^{238}U$	± 2σ	ρ†	$^{207}Pb/^{206}Pb$	± 2σ	$^{208}Pb/^{206}Pb$	± 2σ	$^{208}Pb/^{232}Th$	± 2σ	$^{232}Th/^{238}U$	± 2σ	$^{207}Pb/^{235}U$ age	± 2σ Ma	$^{206}Pb/^{238}U$ age	± 2σ Ma	$^{207}Pb/^{206}Pb$ age	± 2σ Ma	$^{208}Pb/^{232}Th$ age	± 2σ Ma	^{208}Pb-corr. age§	± 2σ Ma	^{207}Pb-corr. age§	± 2σ Ma	f_{206}‡	f_{208}‡
Durango	0.4630	0.1336	0.0094	0.0027	0.90	0.4453	0.0576	4.0640	0.5833	0.0019	0.0003	17.0843	0.7573	386.3	92.7	60.4	17.0	4069.7	192.4	38.2	6.0	24.6	14.3	30.0	9.7	0.50	0.26
	0.3102	0.1211	0.0075	0.0037	0.95	0.3708	0.0647	5.3998	1.0293	0.0016	0.0004	18.6995	1.8211	274.4	93.9	48.1	23.9	3794.9	264.3	32.2	7.4	23.7	17.2	28.4	14.7	0.41	0.16
	0.4033	0.1069	0.0096	0.0031	0.93	0.3356	0.0419	3.4444	0.5363	0.0017	0.0004	17.3929	1.8682	344.0	77.4	61.8	20.1	3642.7	191.2	33.3	7.1	16.3	16.9	39.3	13.3	0.37	0.22
	0.1265	0.0370	0.0049	0.0016	0.85	0.2332	0.0393	7.5405	1.2430	0.0016	0.0004	20.0361	1.1483	121.0	33.4	31.4	10.0	3074.1	269.2	32.1	7.3	32.4	11.8	24.0	7.8	0.24	0.06
	0.1612	0.0604	0.0073	0.0021	0.96	0.2487	0.0325	5.4119	0.6780	0.0017	0.0003	18.9292	1.1823	151.8	52.8	47.2	13.4	3176.5	206.8	34.4	5.6	27.6	11.0	35.2	10.2	0.26	0.10
	0.1422	0.0439	0.0075	0.0024	0.80	0.2075	0.0411	5.0060	0.9275	0.0015	0.0002	19.5051	0.9815	135.0	39.0	48.4	15.3	2886.3	321.6	30.0	4.9	20.9	10.7	38.6	12.5	0.20	0.08
	0.2159	0.0546	0.0066	0.0019	0.90	0.2549	0.0325	4.7513	0.6506	0.0018	0.0003	19.1950	1.1390	198.5	45.6	42.7	12.4	3215.3	201.3	35.9	6.2	32.4	11.4	31.5	9.3	0.26	0.11
	0.2735	0.1046	0.0080	0.0028	0.88	0.3628	0.0660	4.9420	1.0094	0.0015	0.0003	18.7330	0.7576	245.5	83.4	51.6	17.9	3761.6	276.0	29.7	5.8	18.0	13.1	31.0	11.6	0.40	0.17
	0.1595	0.0597	0.0061	0.0024	0.90	0.3018	0.0519	6.5187	0.9671	0.0016	0.0003	19.0452	0.7664	150.3	52.3	39.0	15.4	3479.6	266.2	32.5	5.5	29.1	11.6	26.5	10.8	0.32	0.10
	0.1528	0.0481	0.0066	0.0025	0.92	0.2114	0.0320	5.3518	0.8253	0.0016	0.0003	19.0423	0.5659	144.3	42.4	42.7	16.3	2916.4	245.3	33.1	5.1	28.1	11.5	33.8	13.0	0.21	0.08
	0.1573	0.0389	0.0063	0.0020	0.74	0.2380	0.0514	5.6127	0.8637	0.0016	0.0004	16.6705	0.7029	148.3	34.1	40.8	13.0	3106.9	344.0	32.1	7.7	26.6	15.1	30.9	10.3	0.24	0.09
60x60µm	0.1867	0.1782	0.0073	0.0023	1.51	0.3049	0.0958	5.3333	0.8423	0.0016	0.0003	17.5941	0.3561	173.8	152.5	46.6	14.7	3495.3	485.9	32.1	5.7	23.6	12.5	31.4	11.4	0.33	0.13
"	0.2148	0.1475	0.0073	0.0032	0.97	0.3301	0.0914	5.6083	0.8999	0.0016	0.0003	17.4778	0.3994	197.5	123.3	47.0	20.7	3617.6	424.4	31.9	5.7	23.0	15.3	30.2	14.4	0.36	0.13
"	0.1515	0.0625	0.0057	0.0023	0.92	0.2279	0.0376	5.3572	0.4845	0.0016	0.0002	17.8169	0.4554	143.3	55.1	36.5	14.5	3037.6	264.5	32.5	3.5	30.2	10.0	28.1	11.3	0.23	0.09
"	0.1104	0.0558	0.0062	0.0015	1.12	0.1405	0.0288	5.2415	0.5207	0.0015	0.0002	17.9309	0.4801	106.3	51.0	39.7	9.5	2233.4	354.2	31.2	3.9	26.3	8.1	35.0	8.5	0.12	0.05
"	0.2074	0.0784	0.0087	0.0050	1.02	0.3162	0.0542	5.3584	0.5888	0.0018	0.0006	17.7519	0.6808	191.4	66.0	55.7	31.9	3551.4	263.8	36.3	12.6	25.0	27.2	36.8	21.5	0.34	0.13
"	0.0371	0.0178	0.0053	0.0016	0.94	0.0698	0.0155	6.7645	1.1697	0.0015	0.0002	17.5025	0.3968	37.0	17.4	34.1	10.2	922.0	457.7	31.1	4.1	29.3	8.9	33.1	10.0	0.03	0.01
"	0.2232	0.1173	0.0058	0.0017	1.04	0.3548	0.0730	6.2558	0.7296	0.0017	0.0004	17.4570	0.4991	204.6	97.4	37.2	10.8	3727.8	313.0	34.4	8.7	32.8	15.2	22.7	7.5	0.39	0.13
"	0.2742	0.1085	0.0071	0.0016	0.99	0.2685	0.0466	4.9656	0.5828	0.0016	0.0002	17.5401	0.3974	246.0	86.4	45.5	10.3	3297.1	272.2	33.1	4.2	25.8	9.1	32.8	7.9	0.28	0.12
Emerald Lake	1.7858	0.2029	0.0301	0.0040	0.89	0.4509	0.0276	1.3825	0.0863	0.0140	0.0016	2.5358	0.0890	1040.3	74.0	191.2	24.9	4088.1	91.0	280.4	33.0	135.6	46.1	94.9	15.1	0.51	0.76
	1.6490	0.2976	0.0279	0.0053	0.92	0.4428	0.0318	1.3662	0.0829	0.0150	0.0020	2.6203	0.1250	989.2	114.1	177.4	32.9	4061.3	107.0	300.8	39.7	95.5	62.2	89.7	18.8	0.50	0.75
	1.5384	0.2872	0.0287	0.0040	0.94	0.4543	0.0328	1.4673	0.1306	0.0136	0.0021	2.6365	0.1113	945.8	114.9	182.3	25.2	4099.3	107.4	273.9	41.3	121.3	51.1	89.6	15.4	0.51	0.72
	1.5900	0.2459	0.0289	0.0048	0.92	0.4103	0.0259	1.3621	0.0870	0.0175	0.0034	2.5312	0.2236	966.3	96.4	183.5	30.0	3947.2	94.7	351.3	67.2	78.2	67.7	100.4	18.2	0.46	0.69
	1.8112	0.3140	0.0293	0.0053	0.87	0.4716	0.0421	1.4284	0.1199	0.0152	0.0023	2.7415	0.1812	1049.5	113.4	186.1	33.2	4154.7	132.1	305.8	45.2	100.5	67.4	87.4	19.3	0.53	0.77
	1.7032	0.5339	0.0267	0.0090	0.96	0.4660	0.0460	1.4628	0.1362	0.0149	0.0040	2.7695	0.3134	1009.7	200.6	169.9	56.3	4137.0	146.3	299.7	79.6	75.1	116.8	81.0	29.2	0.53	0.75
	1.4533	0.2572	0.0261	0.0061	0.98	0.3916	0.0270	1.3317	0.1093	0.0120	0.0044	2.9518	0.2397	911.3	106.5	166.1	38.1	3877.0	104.0	240.6	87.9	105.5	100.7	94.7	23.0	0.43	0.67
	1.5282	0.2141	0.0293	0.0040	0.86	0.4447	0.0323	1.3352	0.0859	0.0123	0.0017	3.0305	0.1222	941.8	86.0	186.0	25.1	4067.5	108.3	247.6	33.6	133.7	55.2	93.7	15.6	0.50	0.78
	1.4724	0.2274	0.0258	0.0041	0.92	0.4483	0.0279	1.4997	0.0943	0.0139	0.0017	2.9443	0.1218	919.1	93.4	163.9	25.8	4079.5	92.5	278.5	34.3	70.7	56.4	81.8	14.9	0.50	0.70
	1.5715	0.2293	0.0251	0.0041	0.93	0.4381	0.0270	1.4132	0.0850	0.0132	0.0016	3.0255	0.1349	959.0	90.5	159.8	25.6	4045.4	92.0	265.5	32.3	69.2	56.9	81.7	14.9	0.49	0.72
	1.5817	0.2197	0.0295	0.0059	0.97	0.4475	0.0326	1.4401	0.0998	0.0146	0.0022	2.7165	0.1746	963.0	86.4	187.4	37.2	4076.8	108.5	293.1	43.2	113.2	71.7	93.8	20.9	0.50	0.72
	1.7407	0.2494	0.0281	0.0048	0.94	0.4668	0.0286	1.4909	0.0998	0.0161	0.0023	2.6541	0.1653	1023.7	92.4	178.4	30.0	4139.7	91.0	323.7	46.1	79.8	61.5	84.9	16.5	0.53	0.73
	2.0348	0.3913	0.0349	0.0094	0.99	0.4448	0.0375	1.3908	0.1219	0.0204	0.0044	2.6004	0.3165	1127.2	130.9	221.3	58.6	4067.8	125.5	407.7	88.5	99.5	117.9	111.7	32.2	0.50	0.74
	1.5890	0.1952	0.0344	0.0060	0.97	0.3911	0.0249	1.3293	0.0974	0.0158	0.0023	2.9057	0.1397	965.9	76.6	218.1	37.5	3875.1	95.8	317.4	45.3	140.1	77.3	124.8	23.3	0.43	0.67
	1.5384	0.2205	0.0299	0.0061	0.98	0.4077	0.0293	1.3940	0.1045	0.0180	0.0041	2.6972	0.1750	945.9	88.2	190.0	38.5	3937.6	107.8	360.6	82.4	70.9	89.9	104.6	23.0	0.45	0.67
	1.6827	0.3106	0.0306	0.0052	0.92	0.4006	0.0288	1.3513	0.0913	0.0163	0.0028	2.8046	0.1393	1002.0	117.6	194.2	32.7	3911.2	108.3	326.1	55.8	96.2	72.4	108.7	20.3	0.44	0.68
	1.8328	0.3089	0.0265	0.0038	0.88	0.4798	0.0391	1.4779	0.0856	0.0139	0.0016	2.9110	0.1476	1057.3	110.7	168.7	23.6	4180.4	120.6	278.4	31.9	81.3	51.2	77.4	14.6	0.54	0.76
	1.6514	0.2905	0.0274	0.0058	0.91	0.4713	0.0434	1.5241	0.1120	0.0147	0.0022	2.9055	0.1590	990.1	111.3	174.1	36.7	4153.7	136.4	295.7	43.6	77.5	76.6	81.8	20.5	0.53	0.73
	1.5083	0.2274	0.0254	0.0044	0.92	0.4335	0.0294	1.4163	0.0942	0.0138	0.0023	2.9700	0.1792	933.7	92.1	161.8	27.7	4029.7	101.1	276.5	46.6	67.0	65.9	83.7	16.2	0.49	0.71
60x60µm	1.4218	0.1587	0.0296	0.0039	0.90	0.3819	0.0223	1.4898	0.1084	0.0139	0.0018	2.4667	0.1826	898.1	66.5	188.2	24.5	3839.4	88.0	279.4	35.6	133.7	45.6	109.7	15.9	0.42	0.59
"	1.6351	0.1804	0.0282	0.0033	0.92	0.4475	0.0201	1.4465	0.0731	0.0143	0.0014	2.5552	0.1440	983.8	69.5	179.2	20.8	4077.0	66.9	286.1	27.2	111.3	39.4	89.6	12.4	0.50	0.72
"	1.6373	0.2413	0.0294	0.0041	0.94	0.4620	0.0233	1.4374	0.0728	0.0156	0.0021	2.4493	0.2642	984.7	92.9	186.8	25.5	4124.3	74.9	313.6	42.7	111.6	50.5	90.0	14.5	0.52	0.75
"	1.4995	0.1768	0.0273	0.0027	0.92	0.4311	0.0203	1.5056	0.0768	0.0146	0.0017	2.5679	0.1393	930.2	71.8	173.7	17.2	4021.1	70.3	292.1	33.5	97.8	36.9	90.4	11.0	0.48	0.66
"	1.5956	0.1736	0.0272	0.0032	0.90	0.4357	0.0223	1.5143	0.0815	0.0152	0.0016	2.5916	0.1229	968.5	67.9	173.1	20.0	4037.1	76.4	305.8	32.7	86.5	41.1	89.1	12.3	0.49	0.67
"	1.6917	0.2221	0.0279	0.0057	1.07	0.4328	0.0181	1.5987	0.0846	0.0165	0.0018	2.4779	0.4110	1005.4	83.8	177.4	35.7	4027.0	62.5	330.5	36.1	84.6	67.5	92.0	19.7	0.48	0.63
"	1.5688	0.1722	0.0272	0.0028	0.93	0.4527	0.0178	1.3464	0.0540	0.0129	0.0011	2.5838	0.1445	957.9	68.1	173.0	17.6	4094.0	58.4	258.7	23.0	117.6	33.5	85.3	10.7	0.51	0.78
"	1.4946	0.2667	0.0261	0.0041	0.97	0.4575	0.0213	1.3554	0.0778	0.0120	0.0016	2.4870	0.3847	928.2	108.6	166.3	25.8	4109.6	69.3	240.9	31.3	121.1	47.4	81.0	14.2	0.52	0.79
"	1.3848	0.3077	0.0280	0.0033	1.17	0.4144	0.0200	1.4963	0.0750	0.0143	0.0018	2.5784	0.2404	882.5	131.0	178.3	20.5	3962.0	72.3	287.7	35.4	107.9	42.8	96.6	12.8	0.46	0.64
"	1.4380	0.1527	0.0279	0.0037	0.91	0.4086	0.0238	1.4294	0.0911	0.0129	0.0015	2.6257	0.1493	904.9	63.6	177.3	23.5	3941.1	87.5	258.2	29.2	123.8	44.4	97.4	14.7	0.45	0.66
"	1.5271	0.3489	0.0252	0.0051	0.97	0.4784	0.0277	1.5783	0.0873	0.0139	0.0022	2.6140	0.2561	941.3	140.2	160.3	32.2	4175.9	85.8	278.1	43.8	82.3	63.2	73.8	16.6	0.54	0.71
"	1.8190	0.1603	0.0302	0.0033	0.90	0.4644	0.0225	1.5415	0.0886	0.0162	0.0020	2.4933	0.1638	1052.3	57.7	191.7	20.6	4131.9	71.9	325.6	39.5	110.0	42.8	91.8	12.5	0.52	0.71
"	1.7547	0.1979	0.0289	0.0034	0.92	0.4513	0.0213	1.5147	0.0794	0.0164	0.0019	2.4229	0.2373	1028.9	72.9	183.7	21.3	4089.5	70.2	328.5	38.1	99.2	43.5	91.0	12.7	0.51	0.70
"	1.7904	0.1349	0.0293	0.0033	0.99	0.4512	0.0179	1.4871	0.0740	0.0145	0.0015	2.5820	0.1503	1042.0	49.1	185.9	20.5	4089.3	58.9	291.1	29.9	118.1	40.1	92.1	12.1	0.51	0.71
Kovdor	2.3245	0.2441	0.0802	0.0075	0.91	0.2209	0.0098	14.6772	0.4252	0.0193	0.0006	63.7793	1.9699	1219.8	74.6	497.6	44.9	2987.5	71.7	387.2	12.5	374.1	14.9	394.1	37.3	0.21	0.03
	2.7563	0.2962	0.0788	0.0073	0.92	0.2578	0.0110	13.6379	0.4400	0.0189	0.0009	61.1494	2.1845	1343.8	80.1	488.9	43.7	3233.1	67.0	379.3	18.1	365.7	20.9	364.1	34.6	0.26	0.04
	2.1930	0.2214	0.0745	0.0067	0.91	0.2150	0.0090	15.0303	0.4485	0.0189	0.0007	64.8024	2.1686	1178.8	70.4	463.3	40.0	2943.4	67.6	378.7	13.2	368.8	15.3	370.0	33.3	0.21	0.03
	2.4950	0.2856	0.0804	0.0083	0.91	0.2342	0.0113	16.2907	0.5632	0.0192	0.0008	74.1831	2.7398	1270.6	83.0	498.6	49.7	3081.2	77.3	384.8	15.8	373.4	17.9	386.5	40.4	0.23	0.03
	2.2423	0.2204	0.0759	0.0069	0.89	0.2143	0.0096	15.7321	0.4486	0.0189	0.0006	68.2955	2.2498	1194.4	69.0	471.9	41.3	2938.0	72.2	377.7	11.5	367.4	13.5	377.4	34.5	0.21	0.03
	2.1285	0.2100	0.0796	0.0078	0.90	0.2088	0.0090	15.4925	0.5257	0.0192	0.0006	65.5115	2.1846	1158.1	68.2	493.6	46.5	2896.6	69.6	383.5	12.1	370.8	14.4	398.5	39.1	0.20	0.03
	2.0012	0.1972	0.0728	0.0071	0.89	0.2052	0.0092	16.6118	0.5722	0.0185	0.0006	69.6271	2.2399	1115.9	66.7	452.8	42.7	2868.2	73.3	369.9	12.9	361.0	14.9	367.1	35.9	0.19	0.02
	2.1281	0.2334	0.0820	0.0095	0.92	0.2146	0.0096	14.7049	0.4879	0.0189	0.0008	64.1555	2.3238	1158.0	75.8	507.8	56.4	2940.7	72.1	378.7	16.0	363.5	19.0	406.5	46.8	0.21	0.03
	2.3488	0.2777	0.0829	0.0105	0.93	0.2240	0.0101	13.7308	0.4790	0.0193	0.0010	59.6149	2.2674	1227.2	84.2	513.7	62.6	3009.9	72.5	387.1	19.2	370.8	23.0	405.1	51.2	0.22	0.03
	2.4163	0.2731	0.0804	0.0076	0.93	0.2354	0.0098	14.3904	0.4492	0.0185	0.0008	63.2516	2.5218	1247.5	81.2	498.6	45.5	3088.9	66.5	371.4	16.7	356.1	19.3	385.8	37.0	0.23	0.03
	2.3014	0.3047	0.0762	0.0083	0.95	0.2232	0.0101	16.1255	0.5090	0.0191	0.0010	70.0093	2.7220	1212.7	93.7	473.7	49.4	3004.1	72.7	381.9	19.9	372.1	22.4	373.4	40.6	0.22	0.03
	2.0139	0.2136	0.0778	0.0067	0.92	0.2032	0.0089	15.9706	0.5089	0.0189	0.0007	68.1470	2.1552	1120.2	72.0	482.7	39.8	2851.7	71.1	378.8	14.2	367.4	16.3	393.0	33.8	0.19	0.02
	2.0657	0.2275	0.0783	0.0062	0.91	0.2111	0.0106	14.8032	0.4654	0.0193	0.0008	65.2341	1.7429	1137.5	75.4	485.8	37.2	2914.3	81.4	386.4	16.6	374.9	18.8	390.7	31.6	0.20	0.03
	2.0785	0.2558	0.0768	0.0065	0.98	0.2042	0.0091	15.4575	0.4421	0.0189	0.0006	67.0349	2.0858	1141.7	84.4	476.9	38.9	2859.8	72.8	377.8	12.7	366.7	14.7	387.6	33.0	0.19	0.03
	2.2831	0.2096	0.0813	0.0092	0.94	0.2232	0.0092	15.1904	0.4768	0.0193	0.0007	66.2950	2.2113	1207.1	64.8	503.8	55.0	3004.2	66.1	386.1	14.1	372.7	16.8	397.7	45.1	0.22	0.03
	2.6715	0.2805	0.0785	0.0080	0.92	0.2471	0.0106	14.4860	0.4793	0.0198	0.0010	62.7357	2.1964	1320.6	77.6	487.1	47.8	3166.0	67.7	395.9	19.7	384.9	22.7	369.4	38.1	0.25	0.04
	2.7191	0.3588	0.0876	0.0107	0.90	0.2474	0.0145	13.7904	0.4806	0.0196	0.0010	60.5081	2.1438	1333.7	97.9	541.5	63.2	3168.4	93.1	392.7	20.8	373.9	24.6	411.4	50.6	0.25	0.04
	2.2253	0.2572	0.0801	0.0069	0.95	0.2205	0.0097	15.5253	0.4291	0.0187	0.0005	68.4102	1.9967	1189.0	81.0	496.5	41.2	2984.2	70.7	373.8	9.7	360.4	11.6	393.5	34.4	0.21	0.03
	2.1296	0.2113	0.0791	0.0077	0.90	0.2228	0.0099	15.2990	0.4573	0.0189	0.0007	64.4635	1.8794	1158.5	68.6	490.5	46.0	3001.1	71.2	378.3	13.1	365.2	15.5	387.2	37.9	0.22	0.03
	2.0091	0.2920	0.0791	0.0078	0.98	0.2071	0.0108	16.2064	0.5044	0.0186	0.0007	69.3792	2.7838	1118.6	98.5	490.8	46.5	2883.4	84.4	371.9	14.7	359.0	16.9	397.3	39.3	0.20	0.02
Mineville	1.8760	0.1068	0.1759	0.0059	1.00	0.0786	0.0018	1.8762	0.0262	0.0514	0.0014	6.5938	0.1315	1072.6	37.7	1044.5	32.1	1162.3	46.3	1012.8	27.5	1243.4	274.2	1039.1	33.5	0.01	0.01
	1.8165	0.0828	0.1669	0.0064	0.94	0.0771	0.0013	1.8174	0.0244	0.0508	0.0016	6.3769	0.1245	1051.4	29.8	994.8	35.1	1124.5	33.3	1001.3	32.5	957.9	299.8	989.3	36.4	0.00	0.01
	1.9284	0.1201	0.1749	0.0070	1.03	0.0796	0.0015	1.9243	0.0235	0.0519	0.0020	7.2108	0.1951	1091.0	41.6	1038.8	38.3	1185.9	38.2	1022.3	39.6	1302.2	742.3	1032.0	39.8	0.01	0.01
	1.8072	0.0895	0.1707	0.0064	0.97	0.0808	0.0013	1.9642	0.0215	0.0507	0.0016	7.2842	0.1552	1048.1	32.4	1015.9	35.0	1217.4	32.3	999.0	32.1	1336.8	720.7	1006.8	36.2	0.01	0.01
	1.9202	0.0831	0.1757	0.0062	0.94	0.0807	0.0012	1.9573	0.0212	0.0517	0.0017	7.2791	0.1302	1088.1	28.9	1043.5	34.2	1213.9	30.3	1019.1	33.2	1443.4	628.2	1035.6	35.5	0.01	0.01
	1.8962	0.0788	0.1795	0.0071	0.92	0.0808	0.0013	1.9279	0.0222	0.0525	0.0018	7.1127	0.1383	1079.8	27.6	1064.1	39.0	1217.3	31.4	1033.5	34.6	1420.3	533.9	1056.8	40.5	0.01	0.01
	1.7238	0.1240	0.1627	0.0064	1.13	0.0774	0.0015	1.9805	0.0253	0.0495	0.0023	7.1993	0.2365	1017.5	46.2	971.9	35.2	1130.6	38.2	975.8	44.4	860.8	1943.0	965.3	36.4	0.01	0.01
	1.7330	0.0845	0.1684	0.0061	0.97	0.0773	0.0012	1.9368	0.0197	0.0495	0.0016	7.2032	0.1490	1020.9	31.4	1003.3	33.5	1130.0	32.0	977.2	32.1	1392.4	577.9	997.9	34.7	0.01	0.01
	1.6775	0.0825	0.1670	0.0073	0.90	0.0778	0.0017	1.9491	0.0266	0.0490	0.0019	7.3735	0.1864	1000.0	31.3	995.4	40.4	1141.7	42.7	967.0	37.7	1551.2	770.5	989.1	41.8	0.01	0.01
	1.7123	0.0792	0.1673	0.0073	0.95	0.0776	0.0011	1.9717	0.0239	0.0512	0.0016	7.2572	0.1563	1013.1	29.6	997.4	40.3	1137.8	29.2	1010.1	32.2	-	-	991.3	41.8	0.01	0.01
	1.7582	0.0842	0.1696	0.0071	0.93	0.0771	0.0014	1.9552	0.0247	0.0515	0.0016	7.4266	0.1646	1030.2	31.0	1009.7	38.9	1123.4	35.4	1014.6	31.0	-	-	1004.8	40.4	0.00	0.01
	1.7559	0.0697	0.1686	0.0066	0.91	0.0774	0.0013	1.9517	0.0219	0.0525	0.0018	7.3155	0.1935	1029.3	25.7	1004.4	36.3	1130.9	33.2	1033.4	34.9	-	-	999.0	37.6	0.01	0.01
	1.7850	0.0862	0.1698	0.0070	0.94	0.0778	0.0014	1.8228	0.0241	0.0524	0.0015	6.8077	0.1927	1040.0	31.4	1011.1	38.3	1141.5	34.8	1031.7	30.3	789.4	671.1	1005.5	39.7	0.01	0.01
Mudtank	15.5317	1.3569	0.2060	0.0253	0.91	0.6106	0.0343	2.0034	0.1036	0.0713	0.0058	5.7208	0.2456	2848.4	83.3	1207.4	135.4	4533.3	81.6	1392.2	112.3	474.0	1072.2	403.9	85.9	0.69	0.72
	16.6393	1.6616	0.2019	0.0245	0.90	0.6444	0.0340	2.0227	0.0927	0.0678	0.0063	6.2078	0.3329	2914.3	95.6	1185.6	131.6	4611.5	76.3	1326.8	122.2	126.7	3058.4	344.2	82.2	0.73	0.76
	16.1830	1.7477	0.1993	0.0249	0.92	0.6153	0.0312	2.0258	0.1180	0.0736	0.0069	5.5263	0.3043	2887.7	103.3	1171.7	133.8	4544.6	73.5	1436.0	134.8	204.6	1165.0	383.9	80.5	0.69	0.72
	16.7621	1.5588	0.2038	0.0256	0.93	0.6090	0.0311	1.8302	0.1006	0.0764	0.0076	4.9805	0.2925	2921.3	89.1	1195.8	137.1	4529.7	74.2	1487.3	148.2	529.4	681.3	402.1	82.7	0.68	0.79
	16.1367	1.3037	0.2040	0.0290	1.02	0.6162	0.0358	1.9279	0.1003	0.0685	0.0075	5.1428	0.2509	2884.9	77.2	1196.8	155.4	4546.6	84.3	1339.2	145.7	859.0	681.1	391.4	90.5	0.69	0.76
	15.8764	1.3865	0.1951	0.0228	0.93	0.6374	0.0305	2.0403	0.0932	0.0740	0.0068	5.8480	0.3195	2869.4	83.4	1149.1	122.9	4595.6	69.1	1443.7	133.4	-	-	343.3	75.7	0.72	0.74
	17.8736	1.7453	0.1912	0.0205	0.90	0.6776	0.0310	2.1031	0.1041	0.0828	0.0085	5.2112	0.3018	2983.0	93.9	1127.7	110.8	4684.0	65.9	1608.0	165.9	-520.2	1537.2	277.7	72.7	0.77	0.77
	17.2644	1.9439	0.2142	0.0327	0.89	0.7031	0.0514	2.0838	0.1370	0.0910	0.0095	5.1435	0.3665	2949.6	108.1	1251.3	173.7	4737.0	105.0	1760.4	183.7	-279.6	1586.8	269.0	109.5	0.80	0.81
	18.1319	1.7501	0.2010	0.0224	0.87	0.6586	0.0359	2.0467	0.1003	0.0878	0.0069	5.4611	0.2819	2996.8	92.9	1180.8	120.5	4642.8	78.7	1701.0	133.7	-	-	321.1	81.9	0.75	0.76
	15.8892	1.4298	0.1822	0.0174	0.90	0.6286	0.0267	2.0721	0.0853	0.0800	0.0079	5.4340	0.2688	2870.2	86.0	1079.0	95.0	4575.5	61.5	1554.9	153.8	-	-	333.1	64.5	0.71	0.72
	16.2069	1.3682	0.2044	0.0225	0.93	0.6140	0.0271	1.9821	0.1009	0.0851	0.0070	5.4826	0.2566	2889.1	80.7	1199.0	120.2	4541.5	64.1	1650.3	135.4	-1022.2	3954.5	395.6	75.6	0.69	0.73
Otter Lake	3.0402	0.1573	0.1716	0.0058	0.98	0.1273	0.0025	2.2068	0.0353	0.0476	0.0013	7.7879	0.1628	1417.8	39.5	1021.1	31.9	2061.6	34.6	940.9	26.3	51.7	493.5	956.9	31.6	0.07	0.07
	2.9610	0.1533	0.1598	0.0075	0.90	0.1286	0.0029	2.1228	0.0420	0.0473	0.0013	6.8171	0.3432	1397.7	39.3	955.6	41.5	2079.3	39.1	933.5	25.2	1165.8	459.3	891.5	40.5	0.07	0.07
	2.9873	0.1986	0.1712	0.0103	0.94	0.1306	0.0030	2.2085	0.0449	0.0466	0.0020	8.0391	0.3504	1404.4	50.6	1019.0	56.8	2106.5	40.9	920.9	39.5	114.1	573.2	950.8	55.5	0.07	0.07
	2.9919	0.1496	0.1736	0.0080	0.93	0.1326	0.0025	2.3722	0.0361	0.0480	0.0013	8.9758	0.2226	1405.6	38.0	1032.1	43.9	2133.3	32.4	948.5	26.1	572.7	247.4	961.2	43.0	0.08	0.07
	2.9969	0.1823	0.1656	0.0088	0.94	0.1338	0.0028	2.4002	0.0393	0.0466	0.0015	8.7594	0.2459	1406.8	46.3	987.8	48.5	2149.0	36.4	919.9	30.2	574.0	302.6	916.8	47.2	0.08	0.07
	3.0390	0.1822	0.1669	0.0065	1.02	0.1353	0.0025	2.3833	0.0317	0.0482	0.0014	8.9066	0.1855	1417.5	45.8	995.0	36.0	2167.7	31.7	952.4	27.4	745.3	231.9	922.2	35.1	0.08	0.07
	3.1188	0.1550	0.1699	0.0074	0.92	0.1358	0.0027	2.3808	0.0337	0.0475	0.0012	8.9557	0.2182	1437.3	38.2	1011.7	40.9	2174.1	34.0	938.6	24.1	605.4	232.5	937.7	39.9	0.08	0.07
	2.9785	0.1560	0.1651	0.0071	0.93	0.1331	0.0027	2.3803	0.0346	0.0478	0.0016	8.7626	0.1964	1402.1	39.8	985.1	39.1	2139.5	35.6	943.7	31.1	723.4	276.5	915.1	38.2	0.08	0.07

	2.9090	0.1460	0.1663	0.0064	0.94	0.1304	0.0024	2.3595	0.0303	0.0479	0.0014	8.6867	0.2382	1384.3	37.9	991.7	35.5	2103.3	32.9	946.5	27.1	694.8	261.4	924.5	34.8	0.07	0.07
	2.6812	0.1585	0.1680	0.0082	0.94	0.1192	0.0026	1.8881	0.0305	0.0493	0.0021	6.9136	0.1810	1323.3	43.7	1000.9	45.2	1944.4	39.0	972.2	42.2	1289.0	566.9	946.5	44.8	0.06	0.07
	2.6156	0.1576	0.1658	0.0091	0.91	0.1211	0.0031	1.8517	0.0397	0.0467	0.0021	6.7108	0.2150	1305.0	44.3	988.7	50.4	1971.8	45.3	922.0	41.5	1454.9	439.3	932.4	49.7	0.06	0.07
	2.7588	0.1483	0.1659	0.0110	0.94	0.1279	0.0032	1.8626	0.0401	0.0485	0.0024	6.7679	0.2407	1344.5	40.1	989.7	61.0	2069.1	43.5	957.9	47.6	1253.0	611.7	925.5	59.6	0.07	0.08
Slyudyanka	2.9521	0.2223	0.0923	0.0055	0.94	0.2297	0.0064	0.8831	0.0236	0.0425	0.0034	1.9840	0.0621	1395.4	57.1	569.1	32.2	3050.2	44.9	841.3	66.7	459.3	54.0	451.0	27.3	0.21	0.51
	2.8812	0.1864	0.0932	0.0056	0.89	0.2375	0.0071	0.9348	0.0257	0.0422	0.0026	2.0147	0.0672	1377.0	48.8	574.3	33.1	3103.5	47.9	836.3	51.6	466.4	52.8	449.7	27.9	0.22	0.50
	2.7483	0.1523	0.0886	0.0045	0.90	0.2302	0.0055	0.9422	0.0234	0.0405	0.0022	2.2407	0.0689	1341.6	41.3	547.1	26.8	3053.8	38.5	802.8	43.1	423.7	46.8	432.9	22.8	0.22	0.48
	2.9878	0.1727	0.0950	0.0053	0.94	0.2384	0.0046	0.9384	0.0187	0.0410	0.0020	2.2283	0.0651	1404.5	44.0	585.2	31.4	3109.1	31.1	811.4	38.9	477.9	51.3	457.9	26.3	0.23	0.50
	2.9914	0.2075	0.0917	0.0051	0.94	0.2421	0.0061	0.9695	0.0231	0.0426	0.0024	2.2061	0.0671	1405.4	52.8	565.6	30.1	3133.9	40.3	843.6	48.1	434.6	51.9	439.6	25.3	0.23	0.50
	3.2063	0.1823	0.0988	0.0050	0.92	0.2435	0.0055	0.9660	0.0210	0.0452	0.0020	2.2019	0.0646	1458.7	44.0	607.1	29.4	3143.0	36.0	893.2	40.2	475.6	49.2	471.7	24.9	0.23	0.50
	3.0211	0.1842	0.0962	0.0055	0.90	0.2408	0.0066	0.9388	0.0235	0.0422	0.0023	2.2751	0.0680	1413.0	46.5	591.9	32.4	3125.4	43.5	835.9	45.9	472.3	55.1	461.5	27.3	0.23	0.51
	3.0435	0.1835	0.0941	0.0061	0.93	0.2417	0.0058	0.9317	0.0226	0.0422	0.0027	2.1628	0.0817	1418.6	46.1	579.5	35.9	3131.1	38.4	835.3	54.0	463.0	59.5	451.0	29.7	0.23	0.52
	2.7937	0.1951	0.0891	0.0050	0.93	0.2425	0.0066	0.9479	0.0213	0.0426	0.0026	2.1711	0.0734	1353.8	52.2	550.1	29.5	3136.2	43.4	843.4	52.0	414.6	51.6	427.0	24.8	0.23	0.51
	3.0117	0.2432	0.0937	0.0057	0.96	0.2502	0.0072	0.9915	0.0238	0.0422	0.0025	2.3444	0.0847	1410.6	61.6	577.4	33.4	3186.3	45.5	836.0	50.1	444.4	59.1	443.3	27.8	0.24	0.51
	3.2692	0.1979	0.0945	0.0061	0.91	0.2592	0.0068	1.0250	0.0293	0.0442	0.0033	2.4079	0.0892	1473.7	47.1	581.8	36.1	3242.0	41.4	874.6	65.7	424.6	68.7	440.4	29.4	0.25	0.51
	3.1449	0.2178	0.0936	0.0065	0.92	0.2461	0.0067	0.9932	0.0284	0.0425	0.0027	2.3940	0.0997	1443.8	53.3	576.8	38.4	3159.9	43.1	840.7	53.7	436.5	68.1	445.7	31.6	0.23	0.50
DC 4/5/2	23.9230	2.6904	0.2577	0.0328	0.94	0.6818	0.0291	1.6760	0.0789	0.6059	0.0848	0.7110	0.0746	3265.3	109.6	1477.8	168.1	4692.9	61.4	9574.2	1339.8	360.7	336.9	352.3	98.2	0.78	0.97
	23.3181	2.4514	0.2447	0.0316	0.94	0.7012	0.0321	1.7535	0.0873	0.5058	0.0654	0.8111	0.0653	3240.3	102.4	1411.1	163.9	4733.2	65.7	8273.3	1069.4	345.1	307.9	298.4	96.7	0.81	0.96
	38.2840	2.9389	0.3950	0.0467	1.01	0.7097	0.0281	1.8609	0.0862	0.9600	0.1005	0.7795	0.0645	3727.3	76.0	2145.8	215.6	4750.5	56.9	13601.8	1423.8	263.0	482.3	451.9	144.6	0.82	0.92
	18.6452	1.9649	0.2071	0.0261	0.95	0.6436	0.0261	1.6208	0.0845	0.4091	0.0543	0.8428	0.0697	3023.6	101.6	1213.2	139.6	4609.7	58.5	6932.3	920.5	302.8	262.8	345.0	77.8	0.73	0.95
	23.4465	2.5378	0.2594	0.0286	0.94	0.6818	0.0261	1.6788	0.0775	0.7791	0.1457	0.5826	0.1007	3245.7	105.4	1486.9	146.1	4692.9	55.1	11644.1	2178.2	291.0	423.2	354.7	92.8	0.78	0.97
	20.7648	2.5479	0.2463	0.0363	0.95	0.6470	0.0308	1.5864	0.0704	0.4302	0.0628	0.8863	0.0752	3127.7	118.9	1419.6	187.7	4617.2	68.9	7232.7	1055.4	457.3	331.8	402.9	101.5	0.74	0.97
	18.0333	1.9608	0.2171	0.0320	0.98	0.6360	0.0289	1.5601	0.0738	0.4265	0.0521	0.7412	0.0587	2991.5	104.6	1266.3	169.3	4592.4	65.7	7179.4	876.8	459.6	264.3	374.1	88.9	0.72	1.01
	18.7928	2.2028	0.2270	0.0342	0.97	0.6425	0.0304	1.5866	0.0779	0.4236	0.0564	0.8373	0.0975	3031.2	113.0	1318.9	179.5	4607.2	68.4	7139.3	950.5	408.3	315.9	379.6	94.4	0.73	0.96
	18.3692	2.1119	0.2081	0.0244	0.93	0.6485	0.0286	1.3348	0.0583	0.3371	0.0452	0.8615	0.0783	3009.3	110.7	1218.4	130.4	4620.6	63.6	5871.0	786.9	491.3	228.8	338.9	78.7	0.74	1.16
	37.6377	5.2841	0.3884	0.0664	0.98	0.7354	0.0307	1.8574	0.0919	0.7237	0.1031	0.9840	0.1163	3710.4	138.9	2115.5	308.4	4801.6	59.8	11005.3	1568.1	349.7	661.9	368.3	154.6	0.85	0.95
	23.7644	2.5033	0.2644	0.0310	0.94	0.6583	0.0271	1.6771	0.0784	0.7369	0.0997	0.6096	0.0562	3258.8	102.6	1512.5	158.2	4642.2	59.4	11159.3	1510.0	341.3	321.7	409.1	97.2	0.75	0.94
	23.1449	3.1012	0.2621	0.0359	0.95	0.6971	0.0304	1.7525	0.0762	0.6310	0.1403	0.6851	0.0612	3233.1	130.4	1500.7	183.4	4724.7	62.7	9887.1	2324.5	384.8	431.1	327.7	102.5	0.80	0.95

[a] ρ refers to an error correlation algorithm that employs the uncertainties on the U-Pb isotopic data uncorrected for common Pb, where $\rho = [(err\ ^{207}Pb/^{235}U)^2 + (err\ ^{206}Pb/^{238}U)^2 - (err\ ^{207}Pb/^{206}Pb)^2] \div [2 \times (err\ ^{207}Pb/^{235}U) \times (err\ ^{206}Pb/^{238}U)]$. [b] ^{207}Pb- and ^{206}Pb-corrected ages refer to $^{206}Pb/^{238}U$ common Pb-corrected ages assuming $^{207}Pb/^{235}U$ - $^{206}Pb/^{238}U$ and $^{208}Pb/^{232}Th$ - $^{206}Pb/^{238}U$ concordance respectively. [c] f_{206} and f_{208} refer to the $^{206}Pb_{common}$ / $^{204}Pb_{total}$ and $^{208}Pb_{common}$ / $^{206}Pb_{total}$ ratios calculated using equations Eq. (A.8) and Eq. (A.7) respectively in Appendix A.

Table 2

Table 3
Summary of apatite age and concentration data

	Th	U	Pb	Th/U	n	$^{208}Pb/^{206}Pb_i$	$^{207}Pb/^{206}Pb_i$	TW anchored	MSWD	2σ %	TW Concordia	MSWD	2σ %	^{207}Pb-corr. average	MSWD	2σ %	^{208}Pb-corr. average	MSWD	2σ %
Durango	556	31.7	1.00	17.5	19	2.06793	0.83771	32.3 ± 2.4 Ma	0.69	7.4%	34.3 ± 5.4 Ma	0.69	16%	30.6 ± 2.3 Ma	0.82	7.6%	*32.5 ± 1.2 Ma	0.50	3.7%
Emerald Lake	122	47.2	3.22	2.58	33	2.07250	0.84186	92.5 ± 3.3 Ma	1.60	3.6%	260 ± 150 Ma	0.72	58%	90.5 ± 3.1 Ma	1.30	3.4%	105 ± 9.0 Ma	0.57	8.6%
Kovdor Carbonatite	3539	55.7	65.0	63.5	20	2.05591	0.83087	387 ± 8.2 Ma	0.48	2.1%	414 ± 80 Ma	0.48	19%	386 ± 8.2 Ma	0.49	2.1%	*380 ± 3.1 Ma	0.78	0.8%
Mineville	2630	383	187	6.87	13	2.15856	0.91219	1011 ± 15 Ma	1.80	1.5%	883 ± 98 Ma	0.70	11%	1009 ± 15 Ma	1.80	1.5%	*1009 ± 13 Ma	1.60	1.3%
Mudrank	47.3	8.96	5.98	5.27	11	2.09885	0.86486	355 ± 30 Ma	2.00	8.5%	1163 ± 750 Ma	0.63	64%	349 ± 31 Ma	2.00	8.8%	459 ± 370 Ma	0.67	81%
Otter Lake	1487	195	96.1	7.64	12	2.14650	0.90309	933 ± 12 Ma	1.00	1.3%	986 ± 140 Ma	1.05	14%	932 ± 12 Ma	1.01	1.2%	*941 ± 8.5 Ma	0.74	0.9%
Slyudyanka	202	94.2	17.6	2.14	12	2.09885	0.86486	448 ± 7.3 Ma	1.07	1.6%	424 ± 130 Ma	1.16	31%	447 ± 7.3 Ma	1.05	1.6%	450 ± 15 Ma	0.70	3.4%
DC 4/5/2	7.28	9.89	7.55	0.74	12	2.08900	0.85700	364 ± 21 Ma	1.04	5.8%	314 ± 87 Ma	1.02	28%	361 ± 27 Ma	0.56	7.6%	390 ± 92 Ma	0.22	24%

All errors are quoted at the 2σ level. TW anchored denotes a Tera-Wasserburg lower intercept age anchored through $^{207}Pb/^{206}Pb_i$. TW Concordia denotes a Tera-Wasserburg lower intercept age with no initial Pb constraints. The weighted average ^{207}Pb-corrected and ^{208}Pb-corrected ages (^{207}Pb-corr. average and ^{208}Pb-corr. average) use the $^{207}Pb/^{206}Pb_i$ and $^{208}Pb/^{206}Pb_i$ values respectively in the common lead corrections. ^{208}Pb-corrected ages denoted with an asterisk are instead uncorrected $^{208}Pb/^{232}Th$ ages with high Th/U and high Th concentrations.

Table 3

Table 4

Summary of ^{208}Pb- and ^{207}Pb-corrected apatite ages from sample DC 4/5/2 corrected using i) the Pb isotopic composition derived from co-magmatic K-feldspar and ii) an iterative approach based on Stacey and Kramers (1975).

i) Pb corrected using K-feldspar					ii) ^{208}Pb-corrected using iteration							ii) ^{207}Pb-corrected using iteration						
^{208}Pb-corr.	±	1σ Ma	^{207}Pb-corr.	± 1σ Ma	Iter. 1*	Iter. 2	Iter. 3	Iter. 4	Iter. 5	± 1σ Ma	% diff.	Iter. 1*	Iter. 2	Iter. 3	Iter. 4	Iter. 5	± 1σ Ma	% diff.
360.7	±	168.4	352.3	± 49.1	401.6	365.5	363.6	363.5	363.5	± 168.2	0.8%	427.3	364.0	357.2	356.4	356.4	± 49.2	1.1%
345.1	±	154.0	298.4	± 48.4	384.6	348.9	347.1	347.0	347.0	± 153.8	0.5%	372.2	304.1	296.8	296.1	296.0	± 48.4	-0.8%
263.0	±	241.1	451.9	± 72.3	337.0	265.5	258.8	258.1	258.1	± 241.5	-1.9%	570.7	495.3	482.3	480.0	479.6	± 72.5	5.8%
302.8	±	131.4	345.0	± 38.9	336.3	303.9	302.5	302.5	302.5	± 131.4	-0.1%	401.7	351.8	347.7	347.4	347.4	± 39.0	0.7%
291.0	±	211.6	354.7	± 46.4	334.2	292.4	290.0	289.9	289.9	± 211.8	-0.4%	430.2	366.8	359.9	359.2	359.1	± 46.5	1.2%
457.3	±	165.9	402.9	± 50.8	493.0	465.9	464.6	464.5	464.5	± 165.3	1.6%	470.3	417.6	412.5	412.0	411.9	± 51.0	2.2%
459.6	±	132.1	374.1	± 44.4	488.5	466.4	465.5	465.5	465.5	± 131.8	1.3%	432.6	383.7	379.6	379.3	379.2	± 44.6	1.3%
408.3	±	157.9	379.6	± 47.2	441.8	414.1	412.8	412.8	412.8	± 157.6	1.1%	441.4	390.5	386.0	385.6	385.5	± 47.4	1.5%
491.3	±	114.4	338.9	± 39.3	517.7	498.6	497.9	497.9	497.9	± 113.9	1.3%	396.3	345.3	341.1	340.7	340.7	± 39.4	0.5%
349.7	±	330.9	368.3	± 77.3	420.7	359.9	354.2	353.7	353.7	± 330.6	1.1%	490.6	398.7	382.4	379.5	379.0	± 77.5	2.8%
341.3	±	160.9	409.1	± 48.6	383.7	345.3	343.2	343.1	343.1	± 160.7	0.5%	482.8	426.6	420.6	419.9	419.9	± 48.7	2.6%
384.8	±	215.6	327.7	± 51.2	425.4	390.9	389.0	388.9	388.9	± 215.0	1.1%	406.0	337.5	329.8	328.9	328.8	± 51.2	0.4%
390	±	92†	361	± 27	428	396	394	394	394	± 92	1.0%	431	373	367	366	366	± 27	1.4%

*The first iteration uses a starting estimate of 1 Ga for the Stacey and Kramers (1975) Pb model. Subsequent iterations use the Pb-corrected age in the column to the left. †Last row is comprised of weighted means of the 12 analyses.

Table 4

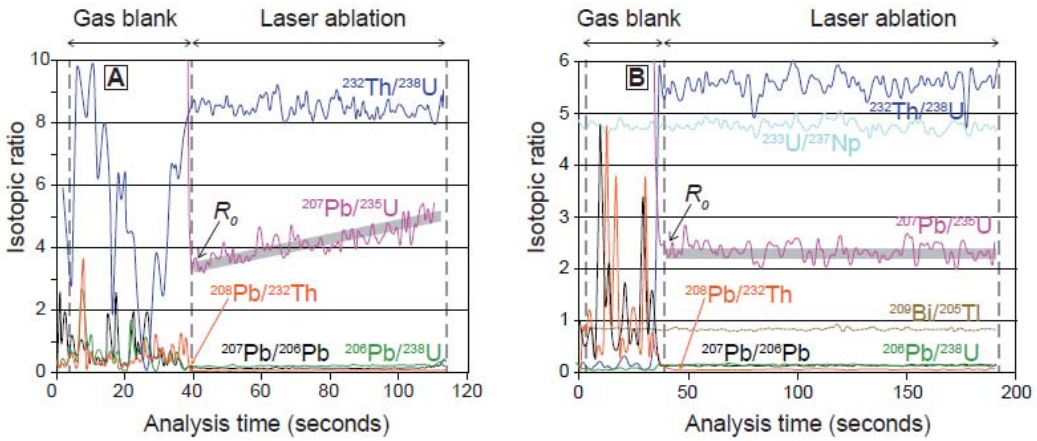

Figure 1

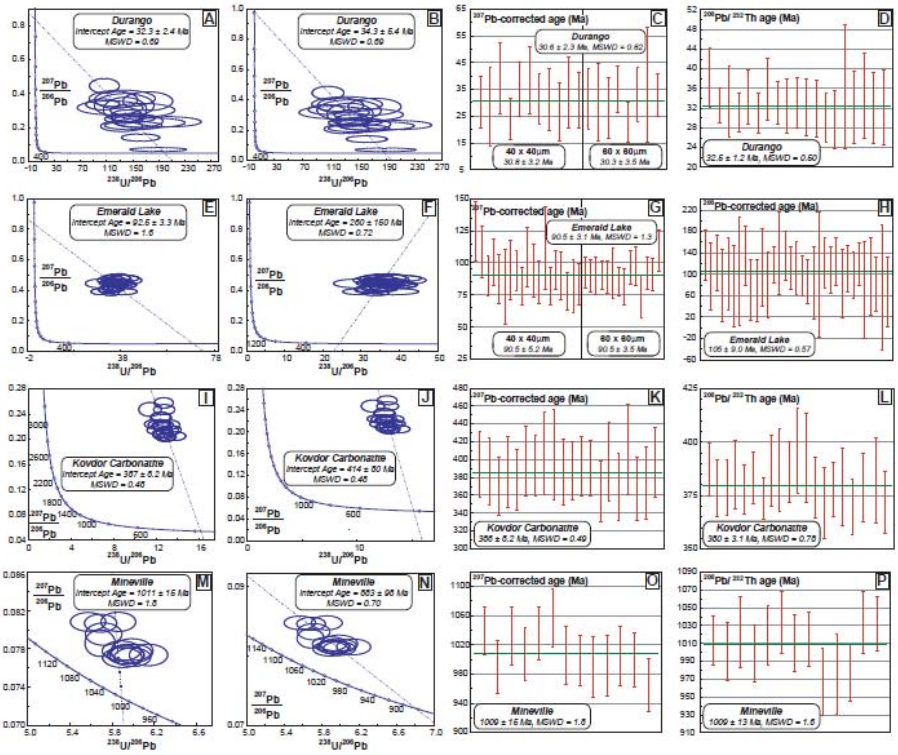

Figure 2A

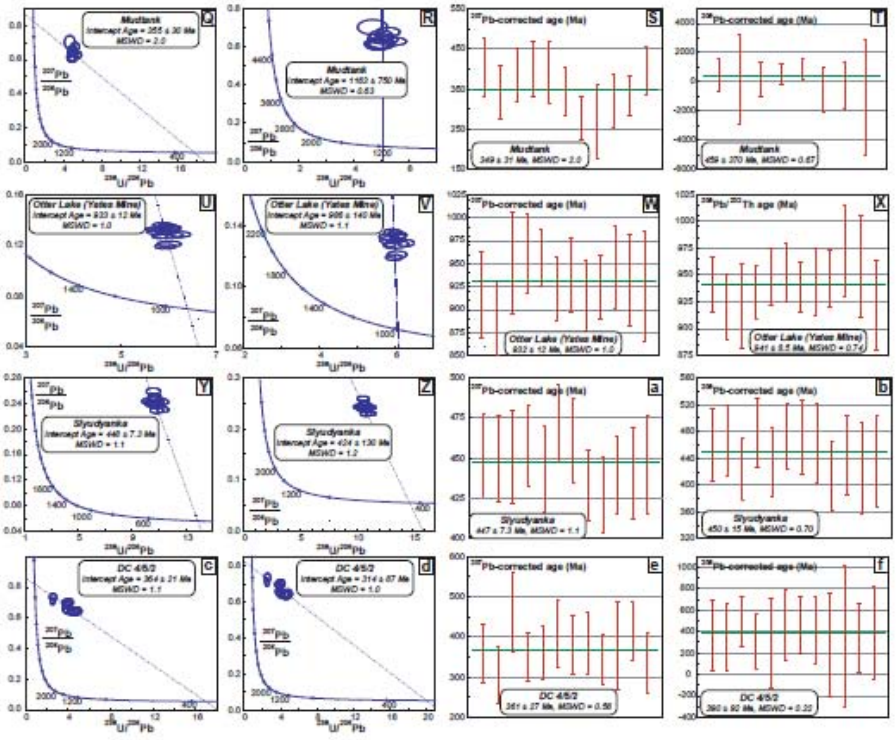

Figure 2B

Research Highlights

- Rapid, accurate U-Pb and Th-Pb apatite dating possible by single collector LA-ICPMS
- Apatite standards yields ages consistent with independent estimates of the U-Pb age
- Th-Pb dating yields much promise, particularly in high Th samples
- Accurate common Pb correction can be achieved without measuring ^{204}Pb
- Opens the possibility of detrital apatite dating for sedimentary provenance analysis